ALKOR-Berichte

***Student Cruise – Marine Geology of the Baltic Sea***

Cruise No. AL546

02.10.2020 – 15.10.2020,
Kiel (Germany) – Kiel (Germany)
GeophysPracUniBremen

**Authors:**
*Master students:*
Andy Forgum Nkemata
Grace Olayanju
Abbass Raza
Nikolas Sanila
Olufemi Soyombo
Alexander Weise
*Bachelor students:*
Florian Böttjer
Carolin Brand
Luca Giere
Alina Ivanova
Yannick Zander

Chief Scientist: Prof. Dr. Volkhard Spiess
University of Bremen, Faculty of Geosciences

2022

**Preface:**

The student training cruise of the Faculty of Geosciences at the University of Bremen took place in 2020 during the Cruise AL 546. However, due to Corona restrictions the course was held in a kind of hybrid mode, in the way that only some advisors sailed, and the content of the cruise was teached to the students in a (online) block course during/after the cruise. This block course was dedicated to master and bachelor students. The master students took part in the frame of the course "Advanced marine geophysical survey project", which is part of the module "Marine Field and Lab Practice" within the internationally oriented postgraduate study program Master of Science "Marine Geosciences". The module is mandatory for students in the first year of the curriculum. The data collected during the cruise are also used for small scientific projects carried out by the students after the cruise. For the bachelor students, the cruise is the "Seegeophysikalische Geländeübung" as part of the module "Projektkurs". This module is mandatory for students in their third academic year. The "Seegeophysikalische Geländeübung" is addressed to students which enrolled the core subject "angewandte Geophysik". Within this core subject, the module "Marine Geophysik" is a major component of the second academic year of the students, and the content communicated in the module „Marine Geophysik" should be applied during the cruise.

During the cruise seismo-acoustic data were collected using a multichannel seismic system, a multibeam system, and the hull mounted echosounders SES2000 and EK60. Additionally, CTD measurements were carried out. Daily reports, data examples and videos/photos were send to the teacher at home and used in the block course. The students became by that acquainted with the acquisition of the data and made typical exercises like survey planning and data analysis.

*As part of the assessment, the students had to write the cruise reports and submit them as a team by one document. It should be noted, that the cruise report is edited by the teachers but could contain still some errors.*

# Table of Contents

# 1 Cruise Summary

## 1.1 Summary in English

The cruise was part of a course in marine geophysics and oceanography at the University of Bremen, and students at the undergraduate and graduate level are required to participate to receive their degree. The data collected also serves the purpose of complimenting the existing data sets, especially the Baltic seismic grid. Thus, the cruise is not only exemplary in terms of teaching the students the different methods of data acquisition, but also provides grounds for expanding the knowledge of the geology in the area. However, from a student's point of view, the cruise serves as a fundamental introduction to the geophysical methods used in marine geological research and provides an opportunity to get hands-on experience with a wide variety of equipment. During the cruise, various data acquisition methods were used. Ship mounted instruments running nearly the full duration of the cruise included: a sediment echosounder (SES), from which image of the uppermost tens of meters of Holocene and glacial deposits, and shallow bedrock, at a high vertical and lateral resolution were obtained, a multibeam echosounder (MBES) with a frequency of 400 kHz, imaging in shallow water the seafloor morphology and measuring roughness, lithology, grainsize, pockmarks and man-made objects (cables, foundations, wrecks) through its backscatter characteristics, an EK60 high resolution echosounder serving the purpose of water column imaging by detecting plankton, fish, sediment suspension and water mass boundaries, CTD casts used to characterize the water properties and Baltic Sea oceanography through measurement of Conductivity, Temperature and Density, and finally High-resolution multichannel seismic (MCS) data would imaging mostly Mesozoic and Cenozoic sediments, including a thin surface cover of glacial and glaciolacustrine deposits in the Kiel Bay, Fehmarn Belt, Mecklenburg Bay, Arkona Basin and Bornholm Basin which would also be useful for seismic inversion.
From a laboratory on board, all instruments were monitored with computer and a variety of software applications, while the participants kept a watch schedule overlooking the data acquisition day and night. As well as monitoring the incoming data. The full duration of the cruise spanned from the 2nd to the 15th of October 2020, with the Kiel bay being the point of start.

## 1.2 Zusammenfassung

Diese Ausfahrt war Teil des Exkursionsmoduls des B.Sc. Geowissenschaften sowie M.Sc. Marine Geoscience der Universität Bremen. Die hierbei gewonnenen Daten ergänzen bereits bestehende Datensätze, insbesondere die seismischen Grids im Bereich der Ostsee. Hintergrund war die Erkundung von Kabeltrassen für einen Windpark. Auf studentischer Seite stand dabei die Einführung in die geophysikalische Methodik sowie die Geologie des untersuchten Gebietes im Vordergrund. Zur Anwendung kamen dabei Sedimentecholot (SES), Fächerlot (MBES), ein EK60 Echolot sowie Mehrkanal-Seismik mit GI-Gun und Streamer. Zusätzlich wurden die Parameter der Wassersäule mittels CTD-Sonde bestimmt. Die Ausfahrt umfasste den Zeitraum vom 2. - 15. Oktober 2020, Start- sowie Zielhafen war Kiel.

# 2 Participants

## 2.1 Principal Investigators

| Name | Institution |
|---|---|
| Prof. Dr. Volkhard Spiess | Uni Bremen |

## 2.2 Scientific Party

| Name | Discipline | Institution |
|---|---|---|
| Prof. Dr. Volkhard Spiess | Chief Scientist | Uni Bremen |
| Dr. Hanno Keil | Marine Geophysics | Uni Bremen |
| Dr. Fenna Bergmann | Marine Geophysics | Uni Bremen |
| Nikolas Römer-Stange | Marine Geophysics | Uni Bremen |
| Opeyemi Ogunleye | Marine Geophysics | Uni Bremen |
| Johanna Pavlak | Marine Geophysics | Uni Bremen |
| Maximilian Meyer | Marine Geophysics | Uni Bremen |

## 2.3 Participating Institutions

Uni Bremen – University Bremen, Faculty of Geosciences

# 3 Research Program

The Alkor AL546 Cruise took place in the Southern Baltic Sea, in the territorial waters of Germany and Denmark. The cruise began on October 2nd from Kiel and ended back in Kiel on October 16th, 2020. The Cruise travelled from the Bay of Kiel (Kieler Bucht), through the Fehmarn Belt and Mecklenburg Bay, to the Arkona Basin area inside the German Exclusive Economic Zone. From there onwards the cruise continued to the vicinity of the island of Rügen and the Prorer Wiek, and then to the Bornholm Basin in the Danish Exclusive Economic Zone of Bornholm island. From the Bornholm Basin the Cruise continued back towards the island of Rügen, and after a short weather standstill between October 13th - 15th in Sassnitz harbour, back to Kiel.

## 3.1 Description of the Work Area

### 3.1.1 Tectonic Evolution

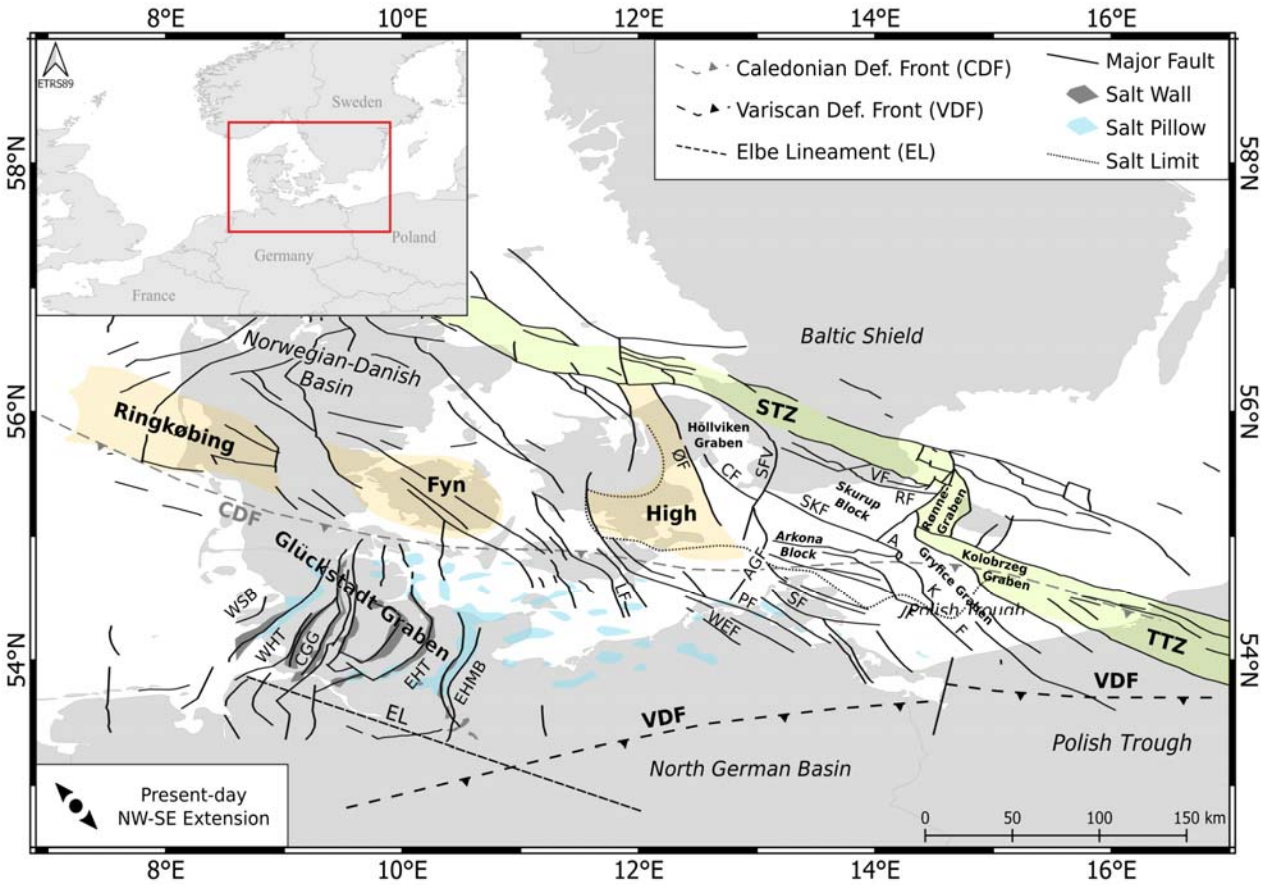


**Fig. 3.1** Tectonic map of the Central European Basin System with the approximate location of the main structures within the study area. AGF: Agricola Fault; AKF: Adler-Kamien Fault; CF: Carlsberg Fault; CGG: Central Glückstadt Graben; EHT: Eastholstein Trough; EHMB: Eastholstein Mecklenburg Trough; JF: Jasmund Fault; LF: Langeland Fault; ØF: Øresund Fault; PF: Prerow Fault; RF: Romeleasen Fault; SF: Samtens Fault; SKF: Skurup Fault; STZ: Sorgenfrei-Tornquist Zone; SVF: Svedala Fault; TF: Trzebiatow

The area of interest for this report concerns a region of the Baltic Sea located between the Baltic Shield to the north, the Norwegian-Danish Basin to the west and the North German Basin to the south (Fig. 3.1). It includes part of the Tornquist Zone, a major fault system

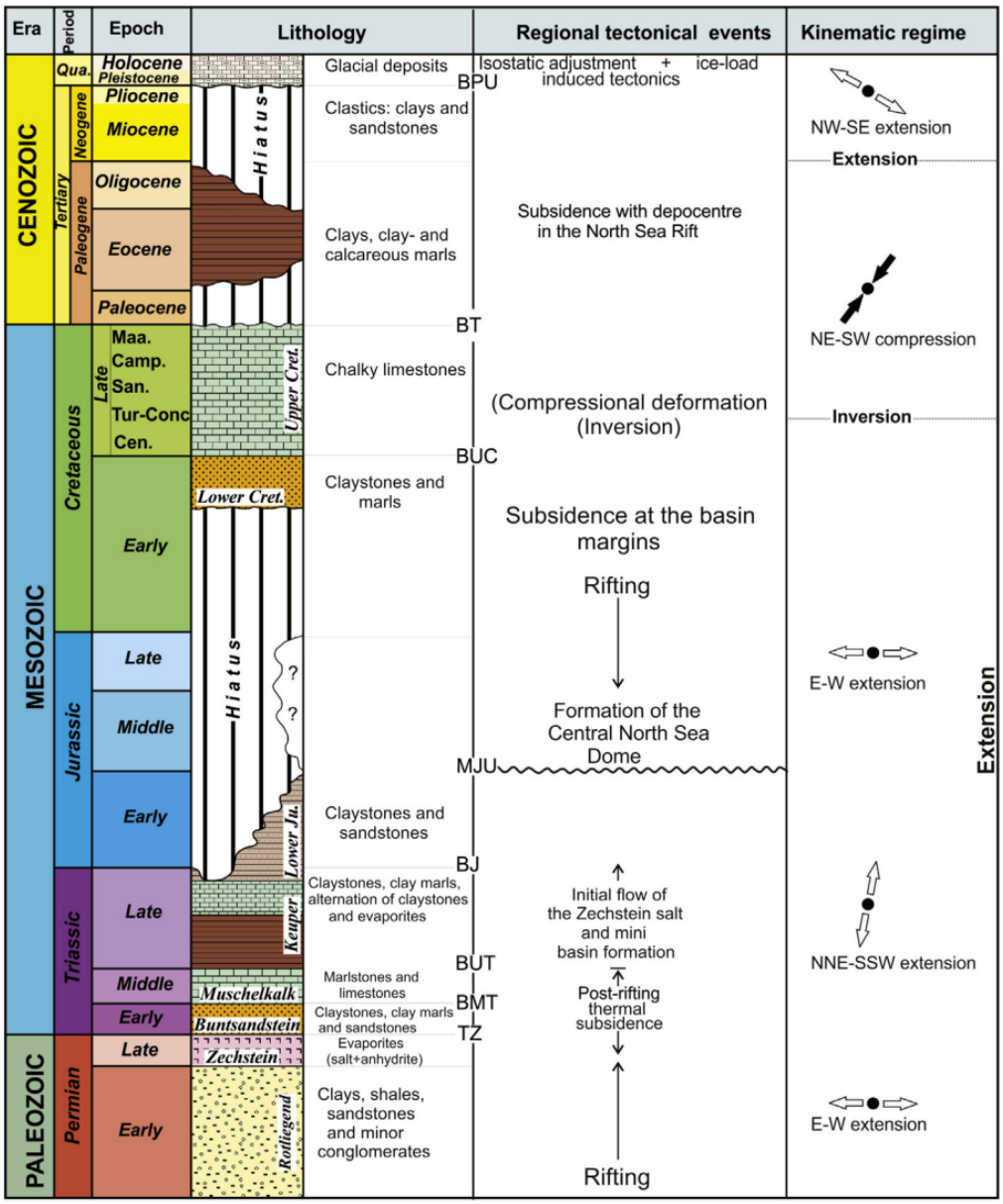


**Fig. 3.2:** Lithostratigraphic table showing the dominant lithologies, main tectonic events and the ages of the major horizons interpreted along thenorthern margin of the North German Basin. BJ: Base Jurassic; BMT: Base Middle Triassic; BPU: Base Pleistocene Unconformity; BT: Base Tertiary; BUC: Base Upper Cretaceous; BUT: Base Upper Triassic; MJU: Mid Jurassic Unconformity; and TZ: Top Zechstein. (Hseinat and Hübscher, 2017)

Fennoscandian Border Zone, which is understood to be the longest pre-Alpine tectonic lineament of Europe. The zone itself consists of two segments, the Sorgenfrei-Tornquist Zone and Teisseyre-Tornquist Zone (Maystrenko et al., 2008).

The area has been influenced by major tectonic events spanning from the Paleozoic until today, including the Caledonian and Variscan Orogenies (Late Cambrian-Late Carboniferous), rifting phases (Early Permian), subsidence during the Mesozoic, Late Cretaceous-Early Tertiary inversion and post-glacial isostatic adjustment since the Late Pleistocene (Fig. 3.2; Hseinat, Hübscher 2017). The Caledonian Orogeny saw the closure of the Tornquist ocean in the Ordovicium-Silurian period, resulting in accretion due to convergence and collision between Avalonia and the passive margin of Baltica. This also lead to the formation of the Caledonian Deformation Front (CDF) (Pharaoh et al.,1997). Variscan orogeny, starting during the late carboniferous, consisted of extension and compressional stress impulses, leading to extensive fracturing of the Upper Devonian-Lower Carboniferous carbonate platform (Krauss, 1994). Fault and graben systems originating in the Permian-Carboniferous period include the – curently active – Adler-Kamien Fault (AKF) (Schlüter et al.,1998) as well as the Vomb Fault, Romeleasen Fault, Agricola-Svedala Fault System, North Rügen Fault, Rønne Graben and the southward half grabens, such as Gryfice Graben and Kolobrzeg Graben which were all formed during extensive phases (Krauss and Mayer, 2004).

Other fault systems like the Wiek Fault, Bergen Fault, Samtens Fault, Stralsund Fault, Prerow Fault or Werre Fault originate from pre-Permian, Variscan and Caledonian fault zones which were reactivated during Triassic and Early Cretaceous times (Krauss and Mayer, 2004). Basement heights like the Ringkøbing-Fyn-High are thought to be caused by a regional tectono-magmatic event in connection with thermal settlement that took place during the Early Permian (van Wees et al., 2000). The Permian itself saw mutliple marine transgression leading to the deposition of marine and non-marine sediments (Rotliegend, Zechstein) (Kossow et al., 2000).

The area comprises three basins which emerged during the Permian-Mesozoic: the North German Basin, the Norwegian-Danish Basin and the Polish Trough (Clausen and Pedersen,1999). Salt structures like the Glückstadt Graben originate in the Middle to Late Triassic, during which a regional E–W directed extension created N-S trending depocentres. Associated features include the Central Glückstadt Graben, the marginal Eastholstein, Westholstein and Hamburg Troughs and the outer Westschleswig and the Eastholstein-Mecklenburg blocks at the flanks (Maystrenko et al., 2008).

Mantle plume activity caused a period of uplift and non-deposition during the Middle Jurassic to Early Cretaceous which resulted in the formation of the central North Sea Dome (Ziegler, 1990). This also led to the removal of parts of the Lower Jurassic and Upper Triassic successions in parts of the area (Kossow et al., 2000). The late Cretaceous saw the collision of Africa-Iberia-Europe which marks the begin of the Alpine Orogeny, leading to contraction and inversion of some basins in the area, but leaving others (like the Glückstadt Graben) unaffected (Grassmann et al., 2005). The Tornquist Zone and adjoining faults were reactivated and inverted accordingly (Maystrenko et al., 2008). Between the Late Eocene and Middle Miocene in the North German Basin, the principal horizontal stress orientation changed from a NE-SW to a NW-SE, the present-day orientation, and oblique to the Glückstadt Graben (Grassmann et al., 2005).

A causative correlation between tectonic evolution of the North German Basin and halokinetics has been suggested, with salt pillows emerging above Triassic fault systems in the Bay of Kiel contrasting the Cenozoic salt movement in the Bay of Mecklenburg (Hübscher et al., 2010). The Quaternary saw at least three extensive glaciation periods, including the last glacial maximum (Elsterian, Saalian, Weichselian).

### 3.1.2 Development of the present Baltic Sea since the Last Glacial Maximum

The development of the Baltic sea during the Quartenary (Pleistocene) is influenced by the recurring glaciation in the northern hemisphere. As a result, the area is subjected to glacial erosion and accumulation. The Baltic sea and adjacent areas have been affected by at least three extensive glaciations, including the Elsterian, Saalian and Weichselian ice sheets (Al Hseinat and Hübscher 2017). The movement of the continental ice sheet resulted in both erosional and depositional features. According to Winterhalter et al., 1981, the effect of the glacial erosion on the morphology of the area is not very pronounced, as a matter of fact, the general topographical outlines of the Baltic sea were established long before the beginning of the Pleistocene glaciation. Only when the glacial flow direction coincided with structurally weak zones in the bedrock, considerable deepening and widening of channels and valleys were caused by glacial gouging (Winterhalter et al. 1981). Glacial deposits such as ground moraines, drumlins, end moraines occur on the bottom of the Baltic sea. The finer material: silt and clay were transported to a greater distance and deposited as varved sediments (Winterhalter et al. 1981).

During the Last Glacial Period (Marine Isotope Stage (MIS) 4 to 2; Fig. 3.3), the Baltic sea basin went through several glaciation events related to the major climatic shifts (Rosentau et al. 2017). During advances and retreats, iceberg calving and freshwater input as well as shifting sea-ice conditions occurred, and the ice sheets recurrently impacted the North Atlantic thermohaline circulation and thereby also the climate of northwest Europe, as indicated by the paleoclimatic records from the North Atlantic Margin and the Greenland ice sheet (Andrén et al. 2011). From detailed correlations and dating of the southwestern Baltic glacial stratigraphy, Houmark-Nielsen and Kjær (2003) and Houmark-Nielsen (2010) reported that the southwest Baltic basin may have experienced two major ice advances during MIS 3, at ca. 50 ka and 30 ka (Figs. 3.3 & 3.4). The coldest phase of the last glacial-interglacial cycle has the largest ice volume, estimated to be equivalent to a sea drop of ca. 120m and is represented by the Last Glacial Maximum (LGM) during the MIS 2, at around 20ka (Fig. 3.5; Lambeck et al. 2010)

After the last deglaciation, the Baltic Sea experienced two lake stages (Baltic Ice Lake and Ancylus Lake) alternating with marine stages (Yoldia Sea and Littorina Sea; Fig. 3.6) (Rosentau et al. 2017).

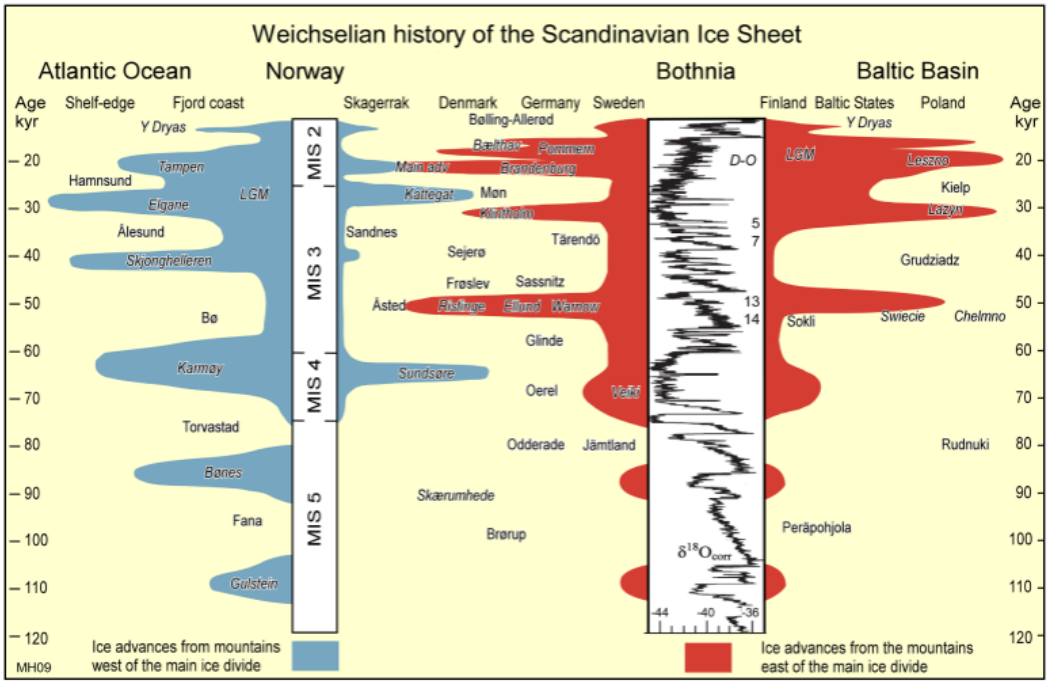


**Fig. 3.3:** Time–distance diagram of the Scandinavian ice sheet during the Last Glacial Period

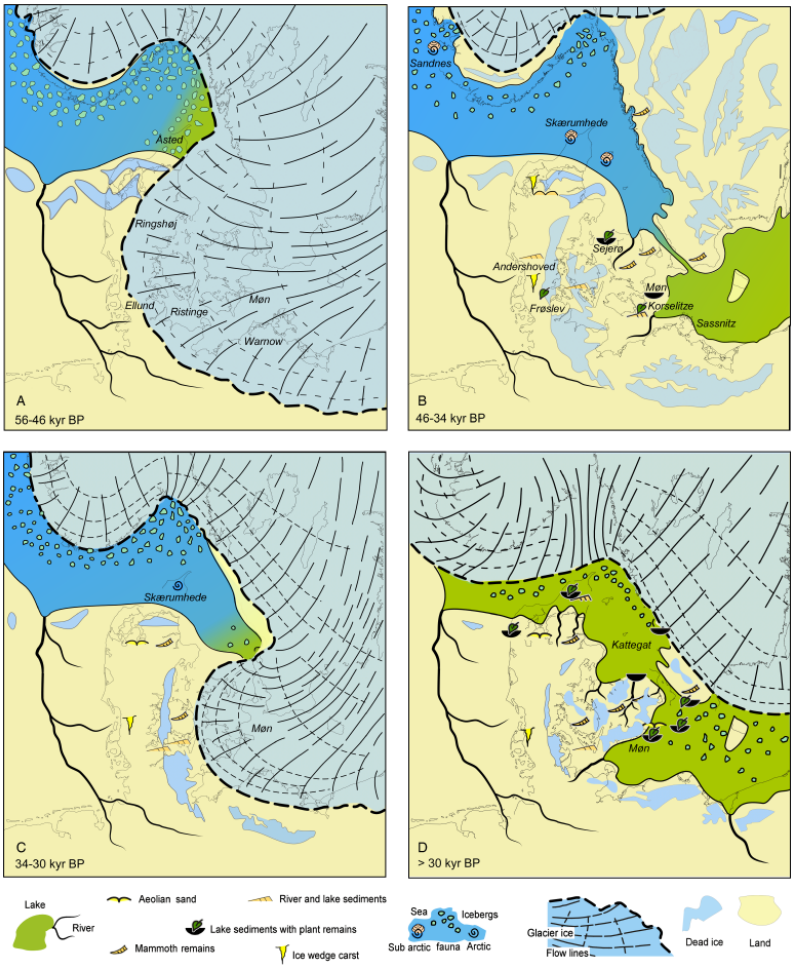


**Fig. 3.4:** Paleogeographical evolution of the southwestern Baltic Sea basin during MIS 3. Houmark-Nielsen (2010). Reproduced with permission from John Wiley & Sons.

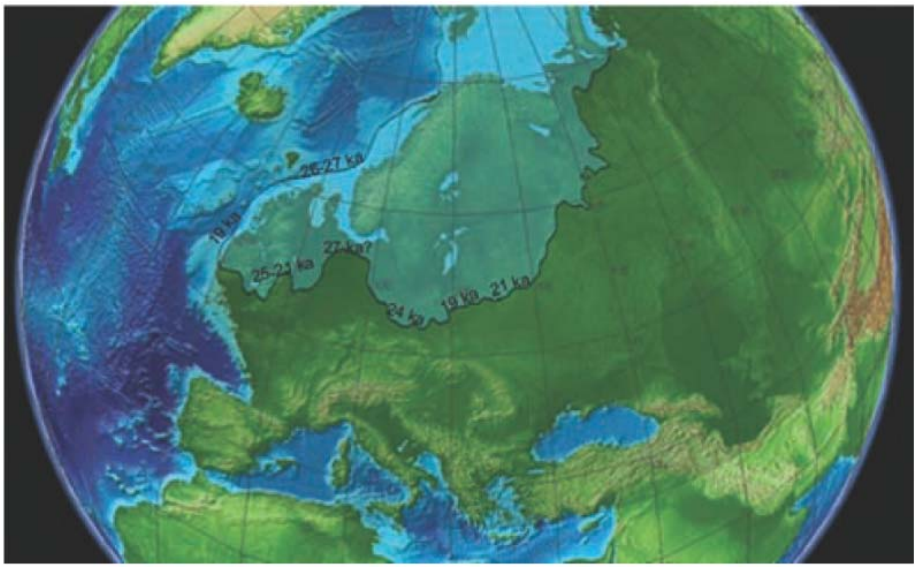


**Fig. 3.5:** Extent of ice sheets (Svendsen et al. 2004) and 120 m lower sea level in northern Europe during the LGM. Note that the maximum glacial limit was reached at different times in different sectors. Topographic data from NASA. Adapted with permission by Rosentau et al. 2017

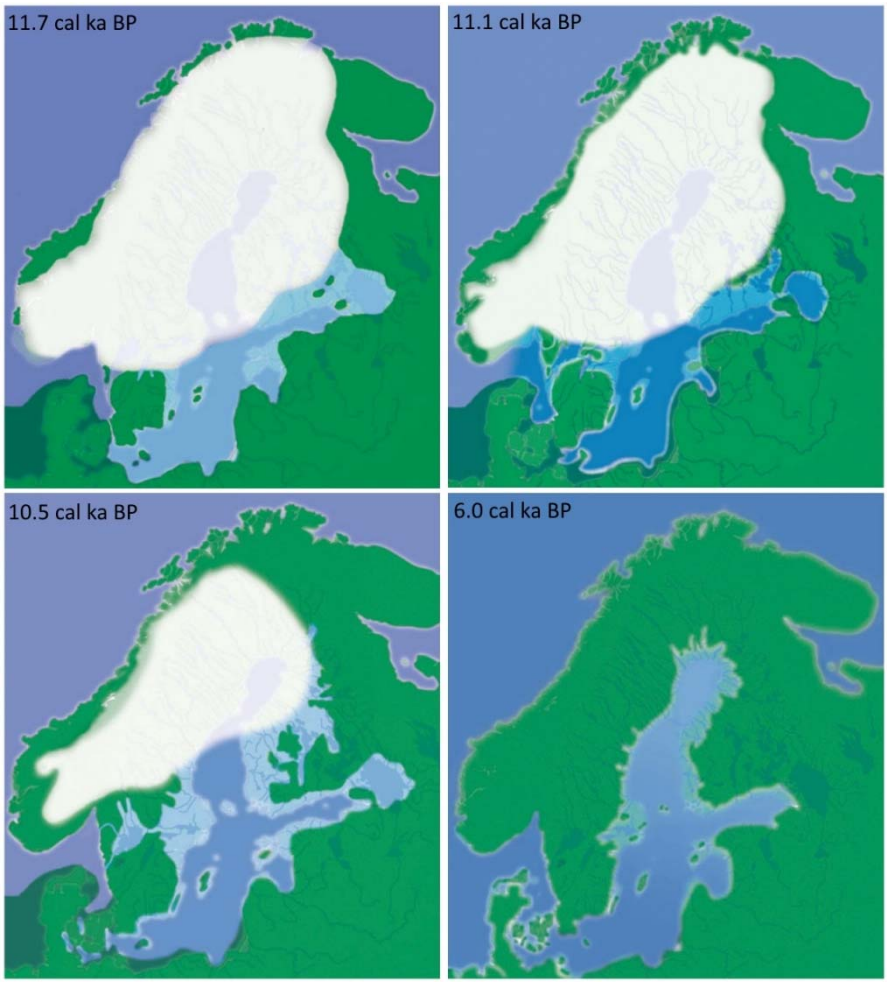


**Fig. 3.6:** Postglacial development of the Baltic Sea basin with alternating lake and marine stages. Andren et al. (2011). Reproduced with permission from Springer Science and Business Media

**Baltic Ice Lake (BIL) (16–11.7 ka BP)**

During the deglaciation of the Baltic Sea basin, a first embryo of the Baltic Ice Lake formed in the southwestern part of the basin approximately 16 ka BP. Rosentau et al. (2017) reported that during the initial stage of the Baltic Ice Lake, it was most likely at the same level as the ocean. However, as the isostatic rebound of the outlet in the Oresund threshold area between Copenhagen and Malmo made up of glacial deposits on top of limestone bedrock was greater than the sea-level rise, the Oresund outlet river eroded its bed in step, at the same pace, with the emerging land. When the fluvial down-cutting reached the flint-rich limestone bedrock, the erosion ceased completely. This is possibly an important turning point in the Baltic Ice Lake development: the uplift of the threshold lifted the level of the Baltic Ice Lake above sea level and the ponding of this large glacial lake started (Bjorck 1995).

As a result of the ice recession in the area immediately north of Mt. Billingen, the first drainage of the Baltic Ice Lake took place at ca. 13 ka BP (Bennike & Jensen 2013). In connection with the Younger Dryas cooling, the ice-sheet margin advanced and the area north of Mt. Billingen was blocked again, causing a second ponding period. At the end of the Younger Dryas, the ice-sheet margin retreated from the threshold at Mt. Billingen, which caused a new sudden lowering of the Baltic Ice Lake level of ca. 25 m down to sea level. This drainage must have had a huge impact on the whole circum-Baltic environment, with large coastal areas suddenly sub-aerially exposed, large changes in fluvial systems, considerable reworking of previously laid-down sediments, as well as the establishment of a large land bridge between Denmark and Sweden (Fig. 3.6) (Rosentau et al. 2017).

Because of the deglaciation, the sedimentation in the BIL was predominantly of a glaciolacustrine character resulting in either glacial varved clay or more homogenous glacial clay: as the ice sheet retreated north the BIL grew with varved clay forming in proximal areas of the ice sheet, while homogeneous clay was deposited in more distal areas. Organic productivity was extremely low and even diatoms were rare (Andrén et al., 2011).

**Yoldia Sea (11.7–10.7 ka BP)**

The onset of the next Baltic Sea stage, the Yoldia Sea (YS), coincides with the base/start of the Holocene Series/Epoch (Walker et al. 2009) and the rapid warming connected with that (Andrén et al. 2011). During the Yoldia Sea stage, saline water entered from the Kattegat through the narrow and shallow straits in the south-central Swedish lowland into the Baltic. The duration of this brackish-water phase was rather short and lasted probably not more than 350 years. Due to the high uplift rate in south-central Sweden, the strait area rapidly became shallower, which together with the large outflow of fresh water prevented saline water from entering the Baltic. The Yoldia Sea was transformed into a huge freshwater lake (Fig. 3.6) (Rosentau et al. 2017).

Apart from being characterized by the rapid deglaciation of the Scandinavian ice sheet, the relative sea level changes of the YS played an important role and were a combination of rapid regression in the recently deglaciated regions and normal regression rates in southern Sweden (1.5–2 m/100 years) (Andrén et al. 2011). At the end of this stage the ice sheet had receded far north and most of today's Baltic Sea basin was deglaciated, apart from the Bothnian Bay. This resulted in sedimentation in the Baltic sea basin where varved glacial clay was deposited in the Bothnian Bay and during the same time postglacial sedimentation in the central and southern part of the basin (Ignatius et al. 1981) The isostatic rebound of the areas around Lake Vänern led to a

situation where the outlets west of Vänern shallowed up and could not "swallow" all outflowing water from the Baltic. This marks the end of the Yoldia Sea. (Andrén et al. 2011).

**Ancylus Lake (10.7–9.8 ka BP)**

When the shallowing up of the outlets west of Lake Vänern forced the water level inside the Baltic to rise, the next stage, the Ancylus Lake (AL), began (Andrén et al. 2011). Rosentau et al. 2017 documented; In the southern part of the Baltic the Ancylus Lake transgression is recorded from submerged pine trees and peat deposits dated between 11.0 ka BP and 10.5 ka BP, whereas areas to the north experienced a continued regression, but at a lower rate than before. The transgression and flooding in the south because of a 'tipping bathtub effect' inevitably resulted in a new outlet in the south.

Since Oresund had been uplifted more than other potential outlet/sill areas farther south, these southern areas were now lower than Oresund. What might now have followed is described by Bjorck et al. (2008). Available data indicate that the Darss sill area, between Germany and Denmark, eventually became the new outlet from the Baltic. However, the transition from the Ancylus Lake to the Littorina Sea is not well understood. For example, there is little evidence for erosion in the German or Danish straits (Lemke et al. 1999; 2001). The sediments of this large freshwater lake are usually poor in organic material, which is partly a consequence of the melt water input to the Baltic from the final deglaciation of the Scandinavian ice sheet and the pristine soils of the mainly recently deglaciated drainage area. Together, this resulted in an aquatic environment with low nutrient input and hence low productivity (Sohlenius et al. 2001; Andrén et al. 2011).

**Initial Littorina Sea (9.8–8.5 ka BP) and Littorina Sea (8.5 ka BP–present)**

Remarkable changes in the Baltic Sea and its ecosystem took place when the freshwater Ancylus Lake was transformed first to a brackish-water stage and later to a marine stage. (Rosentau et al. 2017). Early evidence of saline water ingression into the Baltic basin after the Ancylus Lake stage is documented from the Blekinge archipelago (Berglund et al. 2005) and from the Bornholm basin in the southern Baltic around 9.8 ka cal BP (Andrén et al. 2000; 2011).

In the Danish area the first sign of saline ingression is recorded around 10 ka cal BP (in the northern Oresund; Bennike et al. 2012) and around 8.8 ka cal BP (in the Storebælt & Lillebælt: Bennike et al. 2004b; Bennike & Jensen 2011). Around 8.5 ka cal BP the Baltic Sea became a brackish-water basin with significantly increased primary production (Andren et al. 2011) establishing favorable conditions for human exploitation of marine resources and development of coastal settlements (Jons 2011).

**8.5 (8) ka BP–Present**

The onset of the next stage, the Littorina Sea, is seen as a marked lithological change in Baltic Sea cores. It shows up as a very distinct increase in organic content as well as increasing abundance of brackish marine diatoms (e.g., Sohlenius et al. 2001). It has been discussed if this sudden increase in organic carbon content is exclusively coupled to changes in primary production or if it is partly due to better preservation of carbon during anoxic conditions (Sohlenius et al. 1996).

It has also been proposed that an increase in the secchi depth due to flocculation of clay particles and subsequent rapid sedimentation could attribute to an increased primary production

(Winterhalter 1992). Distribution of trace elements in sediments, especially enrichment of barium and vanadium, is linked to the cycling of organic carbon and imply that increased productivity in the basin caused the rise in organic carbon content (Sternbeck et al. 2000). Due to dating problems, it has not been possible to absolutely date the transition from fresh to brackish water. In general, 14C dates between 8.5 and 8 ka BP are quite common for the onset of this important shift (Sohlenius et al. 1996, Sohlenius and Westman 1998, Andrén et al. 2000a), while the OSL-based age-depth model of Kortekaas et al. (2007) suggests an age of 6.5 ka BP for the same shift in the Arkona Basin. Both 14C ages of bulk sediment and bivalves from the very same core give older ages than the OSL ages, but younger than the expected age of 8.5– 8 ka BP. This discrepancy is difficult to explain unless the shift was not the same as determined in other studies; diatom analysis was not carried out by Kortekaas et al. (2007).

Rising sea level and flooding of the Öresund Strait is believed to be the main mechanism behind the onset of the Littorina Sea; melting of the Laurentide and Antarctic ice sheets over couple of millennia caused a 30-m rise in the absolute sea level (Lambeck and Chappell 2001). Episodic melting events of these ice sheets may explain the so-called Littorina transgressions in the Baltic Sea (e.g., Berglund et al. 2005), which are found in areas south of Stockholm. For example, the rapid sea level rise (4.5 m in a few hundred years) in Blekinge centered at 7.6 ka BP has been ascribed to the final decay of the Labrador sector of the Laurentide ice sheet (Yu et al. 2007).

## 3.2 Aims of the Cruise

The primary objectives of the cruise were to apply multiple geophysical survey methods to image the seafloor and subseafloor in the southern Baltic Sea, for the purpose of identifying geological units, and to reconstruct more of the geological history of the Baltic Sea. Using High-resolution Multichannel Seismic (MCS), Sediment Echosounder (SES), Multibeam Echosounder (MBES), and High resolution echosounder imaging and CTD measurements, the cruise aimed to form a comprehensive understanding of the applications of the different methods to students, and gather relevant data on the geology and water mass properties for further research.

With the data gathered from the cruise the aim is to teach the application of methods, and to investigate the afore mentioned structures and water column properties. More specifically for each method, using the MCS the aim was to image mostly Mesozoic and Ceonozoic sediments, and the more recent glacial and glaciolacustrine sediments over the entire cruise. Using the SES the aim was to image mostly Holocene and glacial sediments at higher resolution than using MCS. Additionally, the SES was used together with MBES bathymetry and backscatter data to image seafloor morphology and to localise man-made structures such as cables, foundations, and wrecks. The MBES backscatter was also used to study the backscatter characteristics of sediments as measure of roughness, lithology and grainsize, as well as the characteristics of pockmarks and man-made objects in the backscatter data. The high-resolution echosounder EK80 and CTD casts aim to image the water column for plankton and fish detection, as well as to identify sediments suspension and water mass boundaries.

## 3.3 Agenda of the Cruise

The first days of the cruise seismo-acoustic measurements were carried out in the Kiel Bay, Mecklenburg Bay and Arkona Basin. After a port call in Sassnitz, measurements were continued on the way to the Bornholm Basin, and within the Bornholm Basin. In both areas the main target were tectonic structures. These survey works were interrupted north of Bornholm by CTD stations, followed by surveying the contouritic deposits northwest of Bornholm and again the tectonic structures between Bornholm and Rügen. After another port call in Sassnitz the ship headed back to Kiel to undertake more seismo-acoustic profiling in the Mecklenburg Bay (Fig. 3.7).

All research activities were conducted in accordance regard to the Declaration of Responsible Marine Research (Appendix 1 in the guideline of ships proposals) and the Code of Conduct for Responsible Marine Research in the Deep Seas and High Seas of the OSPAR Maritime Area (Appendix 2 in the guideline for ships proposals).

Especially, the rules for mitigation measures for the operation of weak seismic and/or hydroacoustic sources (BP, boomer, sparker, MB, SS, SBP, air guns with TPV $\leqslant$ 150 in3 (2.5 litres)) were respected as described in App. 3 of the guidelines for cruise proposals. This includes particularly the marine mammal observation procedure before and during seismic and hydroacoustic surveys.

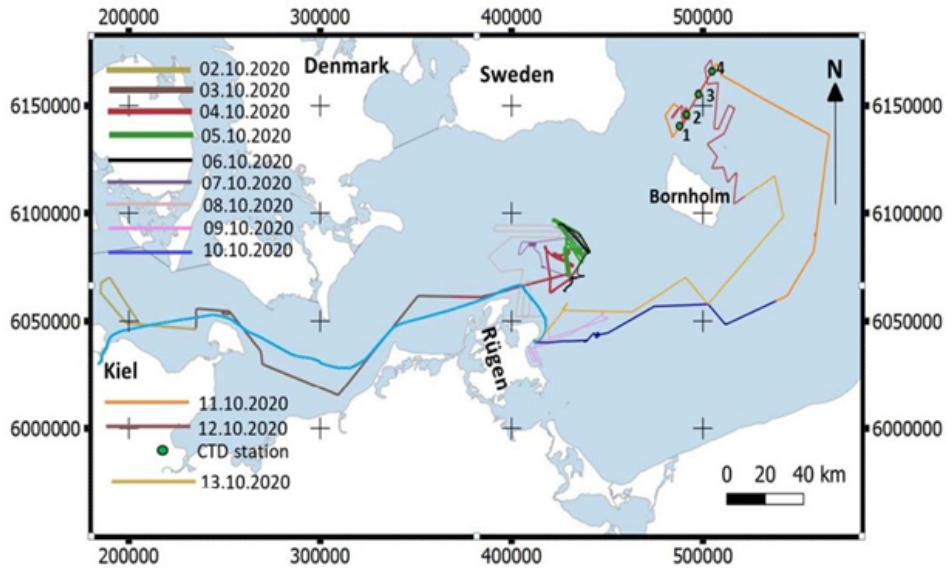


**Fig. 3.7:** Track chart of RV ALKOR Cruise AL546

## 4 Narrative of the Cruise

The cruise set sail on the 2nd of October from Kiel, concentrating on researching the Kiel Bay area. During the transition from harbour, labs were set up and equipment deployed and Multi Beam Echosounder (MBES) calibrated. During the first day the Multi-channel Seismic (MCS) was deployed using the Mini-GI gun with reduced inner volume. After the deployment of equipment survey lines were run in the Kiel Bay. The primary target was imaging salt structures of the Zechstein salt, and salt-related sediment deformation in the subseafloor using MCS. The Sediment Echosounder (SES), MBES, and MCS were all used for data acquisition.

On the 3rd of October the cruise continued from the Kiel Bay, through the Fehmarn Belt into the Mecklenburg Bay. MBES, SES and MCS acquisition continued throughout the day. For far field source signal recordings only single hydrophone data was recorded from between 17:00 and 24:00 UTC, while step-wise changes in air-pressure supply to the min-GI gun were tested between 17:02 and 20:52 to determine appropriate pressures for mammal protection and survey work in vicinity to Natura 2000 areas. The primary objectives for the day were continuing high-resolution MCS surveying of the salt structures and associated deformation, and gathering MCS data on the Werre and Prerow fault systems. MBES and SES were primarily used to survey ripple fields in the area

The cruise continued past the Island of Rügen and into the Arkona Basin on the 4th of October. During the day the mini-GI gun was used in tests on different injector delays. Issues with the trigger delay on the mini-GI gun were noticed and multiple attempts of repair were conducted. In addition to MCS acquisition SES and MBES acquisition was continued, except during the retrieval and redeployment of the mini-GI gun. The primary targets of the day were continuing the MCS survey lines towards the Baltic Shield in the east. Three shorter MCS lines were acquired to assess the subseafloor conditions at a wind-farm area. After testing described above, the MCS surveys

were continued along the Danish border to study glacial deformation, thrusting, and erosion caused by the Scandinavian ice sheet.

The issues with the mini-GI gun continued on the 5th of October despite multiple repair efforts and multiple retrievals and redeployments during the day. MBES and SES acquisition was continued throughout the day with minor brakes during retrievals and redeployments of mini-Gi gun. The primary objective of the day was to survey glacial thrusting and erosion features associated with Quaternary glaciations, and V-shaped subseafloor anomalies of unknown origin possibly related to glacial movements. This was done with dense MCS survey line grid, and of these lines part of them were planned perpendicular to the Quaternary ice movement direction. Additionally, calibration of single-hydrophone was conducted to determine source-receiver offsets and far field source signatures of the GI gun.

On the 6th of October MCS acquisition was continued in the Arkona Basin along the Danish border for imaging of glacial deformation. In the afternoon, after continued issues with airgun causing dropouts and shooting time jumps, the airgun was again retrieved for repairs and MSC surveying was discontinued. After MCS termination for the day, MBES and SES surveys continued on cable sections connecting the wind parks Wikinger and Arkona Südost to land. The primary target was the backscatter characteristics from two buried cable sections. Tests using SES and its beam tilting were conducted to assess the reflections and scatter from the cable sections. This was conducted to study the detection capabilities of acoustic systems in regards to cables.

The cruise continued in the Arkona Basin the 7th of October. The day was commenced with MBES and SES surveying of the power cable area where surveys began on the 6th of October, and of 2 pockmark locations. At the pockmark locations MBES surveying was conducted to determine the existence and nature and size of pockmarks. Additional sites with shallow gas patches were surveyed to localise additional pockmarks from the MBES bathymetry and backscatter data. Water column data was recorded at the pockmark locations to study potential bubble release form pockmarks. In the afternoon MCS work was again commenced with east-west profiles across the northern Arkona Basin along the Danish border, commencing with pre-shooting with lower GI gun pressures for mammal protection. The MCS data was gathered specifically for use in seismic inversion, thus picking targets of particular geological interest and with great physical contrasts. Issues with the mini-GI gun continued.

Survey work as continued in the Arkona basin on the 8th of October, heading southwards towards the east coast of the island of Rügen in preparations for bad weather predicted for the coming days with westerly and north-westerly winds. Survey work was planned to continue in the south in the Prorer Wiek the following day, protected from the winds. During 8th of October MBES and SES data were recorded, while the primary objective was using MCS and single-hydrophone seismic data to survey the deep geology and major fault systems in the subseafloor of the Arkona Basin. Additionally, the data was planned to image post glacial deposits, contourite features, and shallow gas patches in the sediments. The lines heading southward were planned for seismic inversion with major lithological contrasts to be included in the data, such as the boundry of Upper Cretaceous and Quaternary sediments, as well as the boundary of undeformed and deformed Cretaceous. A port call in Sassnitz was schedule for the following day around 1400 UTC for exchange of scientists.

The 9th of October began with continued MBES and SES recording, and MCS data acquisition.

The seismic survey focused on the study of glacial deformation associated with the formation of Jasmund Peninsula as well as the geological history of Prorer Wiek. After retrieval of seismic equipment between 8:41 and 9:11 UTC, MBES and SES surveys were continued. After a short transit to the site of the shipwreck of Jan Heweliusz a MBES survey to image the wreck in terms of bathymetry and backscatter characteristics was conducted. At 10:06 UTC transit towards Sassnitz was began with port call at 12:00 UTC. For the following day departure was planned at 7:00 UTC.

The port of Sassnitz was left at 7:04UTC on the 10th of October, heading east. The first target of the day was the Nord Stream pipeline using MBES and SES. The SES was operated using different beam steering modes at 4 kHz. The survey aimed to assess the size of the pipeline and its precise location, also in regard to burial depth or hight above seafloor. After multiple crossings of the pipeline using MBES and SES; the streamer and mini-GI gun were deployed. The primary objective of the MCS survey was the acquisition of long seismic profiles across the southern Bornholm Basin, imaging the distribution of Cretaceous and older bedrock on the transit from the Arkona Basin into the Bornholm Basin. The seismic survey would also image glacial tills and postglacial sedimentation, to better understand the more recent sedimentation of the southern Baltic Sea. The SES was used for the imaging of late glacial and Holocene muds, where shallow gas was not present. During the day, entry into Danish Exclusive Economic Zone was made.

The cruise continued in the Bornholm Basin on the 11th of October. Surveys were conducted using MBES, SES, and MCS with the mini-GI gun. The objectives of the SES and seismic surveys were to study Post glacial and Holocene sediments, to understand better the different stages of water inflow form the North Sea into the Bornholm Basin. The survey aimed to also image contourite deposits related to the changes in salinity, affecting the density of the water masses during the Baltic Seas evolution.

The survey work continued in the Bornholm Basin in Danish waters on the 12th of October. The days goals were to investigate Quaternary sedimentation, including contourite deposits, in the Bornholm Basin. Additionally, one MCS line was collected to study the internal structure of the water column, as a part of a time series over the last 6 years. This line was complemented with 4 CTD stations to acquire data on the temperature, salinity, and sound velocity of the water column. Surveys were continued throughout the day with MBES, SES and MCS.

On the 13th of October MBES, SE and MCS surveys were continued. The aim of the seismic survey was to acquire long profiles to map contourites as well as to continue the imaging of the distribution of Cretaceous and older bedrock from the Bornholm Basin to the Arkona Basin. This would also show features of the Late Cretaceous inversion reported around the boundary of the two basins. Additionally, quaternary glacial and post-glacial deposits were imaged. Calibration of the seismic signal was conducted to end the seismic survey, using 218 shots. Due to storm warning, and predicted bad weather for the coming day, the cruise continued to Sassnitz harbour, leaving Danish waters, and arriving at 20:57 UTC.

Weather hindered operations on the 14th of October, and port call in Sassnitz continued. Time was used to ensure data was field processed and exported into relevant files for further use. No new geophysical data was acquired during the day. Departure the following morning was planned.

6:30 UTC, the cruise left Sassnitz to conduct geophysical surveys in the Arkona Basin. Bad weather did not facilitate seismic survey operations so transit towards Kiel commenced. During

the transit SES data were recorded imaging mostly Quaternary geology in the uppermost section of the seafloor. Weather conditions improved during the transit, so preparations for leaving the Alkor the following day could begin during transit. Alkor made port at 20:00 UTC

On the 16th of October final cleaning and packing of equipment onto trucks. At 9:00 UTC scientists left from Kiel towards Bremen, ending the AL546 cruise at 12:30 after unloading and stowing gear and data into storage.

# 5 Preliminary Results

## 5.1 Multichannel Seismic (MCS)

### 5.1.1 Measurement Principles

During marine seismic measurements, a seismic source (vibroseis, air gun, sparker, boomer) generates acoustic waves, which propagate with a spherical shape through the water column and the sub-surface. While traveling, the sound wave stimulates the particles it interacts with, resulting in tiny sub-surface vibrations. Variations in the physical properties of different materials in the sub-surface affect the propagation of the sound wave. Different densities and seismic velocities of the materials result in an impedance contrast, which characterises the interface between two different materials. The impedance is the product of density and seismic velocity. According to Snell's law, a sound wave is either reflected or refracted at an interface depending on its angle of incidence and the seismic velocities of the materials. Due to these interactions, the sound wave resurfaces after traveling through the sub-surface and can be recorded by the towed hydrophones. Both the travel time generally referred to as the "two-way travel time" (TWT) and the amplitude of the sound wave are recorded. The raw data then include a signal of the emitted (source) wavelet that is convoluted with the reflectivity of the sub-surface and different types of noise. A few processing techniques can be applied to remove these interfering signals, so that the recorded signal can be transformed into an image of the layers in the sub-surface.

In comparison to single-channel seismic, multi-channel seismic reflection makes use of multiple source-receiver pairs that image the same point of the sub-surface. By using a streamer that contains multiple hydrophone groups, which record a single shot at multiple offsets, many different midpoints between the source and the receivers are generated for every shot. Then, due to the movement of the vessel at a constant speed along the profile, many different source-receiver pairs image the same point on the seafloor and below. All the source-receiver pairs that image the same seafloor mid-point are combined into a common mid-point (CMP) gather. Subsequently, all the traces in a single CMP gather are stacked together to form one trace per CMP. This summation amplifies the signal and suppresses random, incoherent noise, improving the signal-to-noise ratio.

### 5.1.2 Multichannel Seismic (MCS) Data Acquisition

The multichannel surveying unit on board the ALKOR composed of G.I guns, Mini G.I guns, compressor, streamers, birds, and an acquisition system which is this case was the MAMUCS acquisition system.

During the AL546 survey, acquisition of both MCS and single hydrophone seismic data was achieved over a combined profile of approximately 2104 km. Seismic energy with parametric frequencies of 100 kHz and 105 kHz was provided by G.I gun with injector capacity of 25 $in^3$ and micro G.I gun (mini G.I gun with reduced injector volume) of capacity 6 $in^3$, both supplied with compressed air of between 50-140 bars from the compressor. The G.I gun was located 27.47m behind the primary GPS during data acquisition while the mini/micro G.I gun was located some 20.5m behind this same GPS. Shots were fired after every 4 seconds and depending on the scientific objective that was to be achieved, the G.I guns were ran either in true GI mode or harmonic mode.

The G.I gun and mini G.I gun were deployed differently for acquisition of seismic data during the survey. The G.I gun was towered by a crane on the and lowered into the water through the starboard area of the ship (Fig. 5.1). Three umbilicals were connected to this G.I gun, one was for bringing in high pressure compressed air while the other two were for electronic triggers. The G.I gun was attached to a bouy which kept it in a distinct horizontal depth under the water during data acquisition. Meanwhile the mini G.I gun was lowered by hand into the water through the open section of the deck.

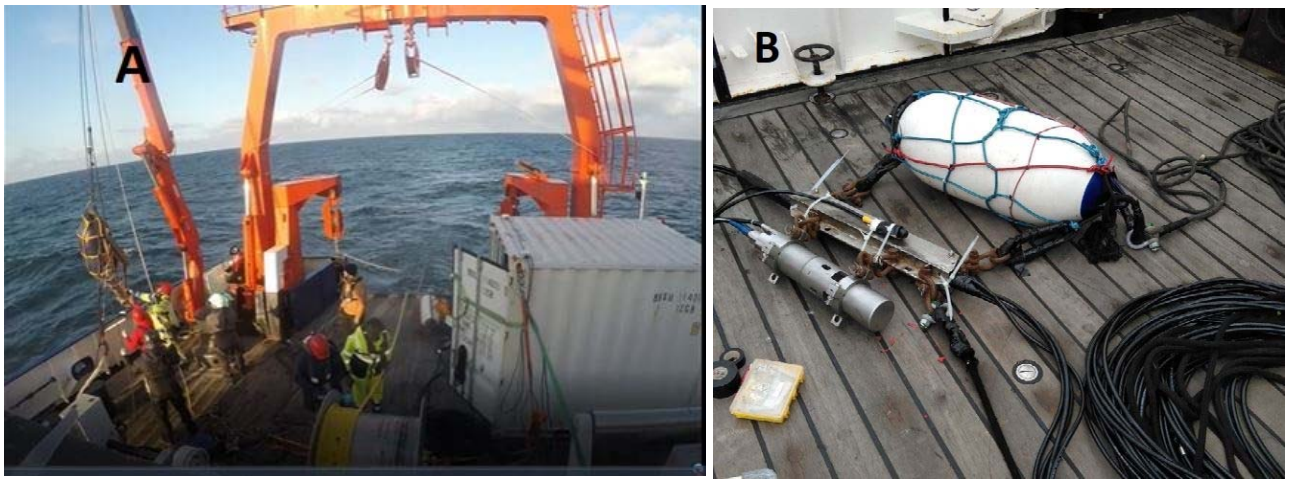


**Fig. 5.1** A) G.I gun being lowered by a crane on the starboard area of ship. B) Umbilicals for compressed air and electronic trigger connected to G.I gun

A towed hydro-acoustic streamer cable (Fig. 5.2) with an active length of 255 m was used to gather data with an initial offset of 1000 meters. Seismic data acquisition was achieved over four profiles (1-18, 18-32, 32-87, 87-108). Channel 1 for the first three profiles was 27.02 m from the primary GPS and 26.70 m for the last profile (see App. 1). Before being lowered into the water, the streamers were attached to depth controlling devices called Birds and then to floatation tubes. These Birds used battery for energy and contained magnetic coils, hence communication with them from the control room was achieved by induction. Collars were attached at the end of every bird. These collars were then used to attach floatation tubes to the birds, the streamers were then attached

to these floatation tubes with the aid of plastic rings around the streamers. So, at the end we had floatation tubes on top and birds beneath the streamers (Fig. 5.2). The assembly of streamer containing GPS, floatation tube and bird was then carefully lowered into the water through the open deck section of the ship.

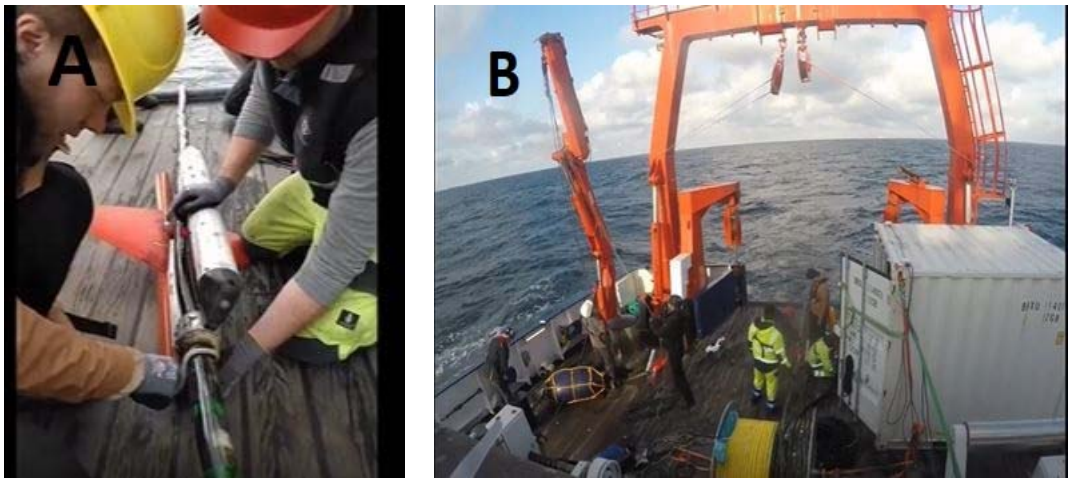


**Fig. 5.2** A) assembly of floatation tube, streamer, and bird (white floatation tube above black streamer and orange bird below) being lowered into the sea. B) Black active portion of streamer being lowered into the sea while yellow inactive remains on streamer drum

Desk cables from the streamer ran through into the control unit (lab) where they were connected to digitalization unit (devices responsible for converting the analog data to digital signals). Connected to this digitalization unit were two monitors showing how raw data is coming in. The first monitor showed data coming from hydrophone of 1m, 2m, and 4m, respectively. With shot a new shot gather appearing after every 4s (Fig. 5.3). The second monitor showed brut stacked unprocessed image of the sea floor and was mainly used for quality control. During this process, there was always a scientist sitting at these monitor checking if the data is coming in correctly and any seismic data that was of interest was immediately printed out and tried to be interpreted by the scientist on board.

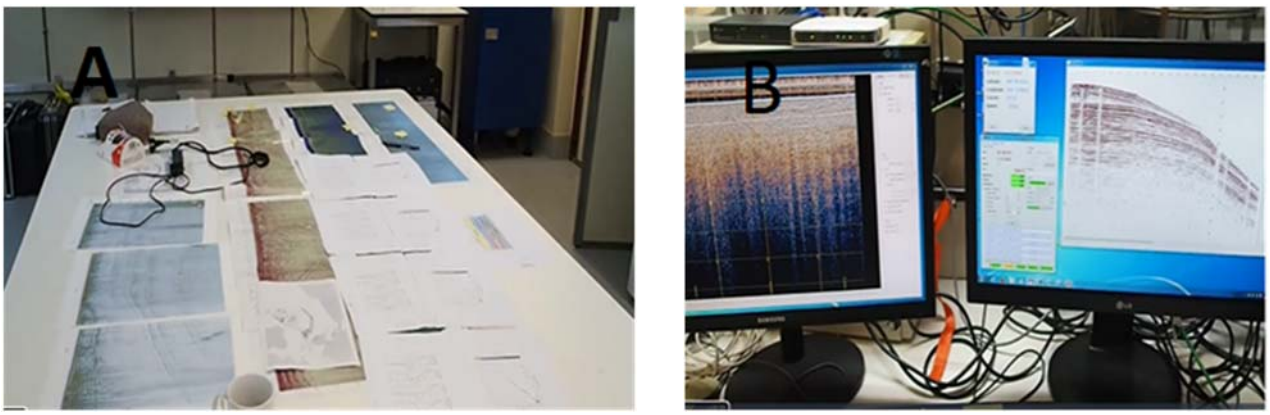


**Fig 5.3:** A) Seismic profiles printed out for check of anything interesting during data acquisition. B) Brute stack unprocessed image of seafloor (left) shot gather from various hydrophones (right).

### 5.1.3 Map of Seismic Profiles Surveyed

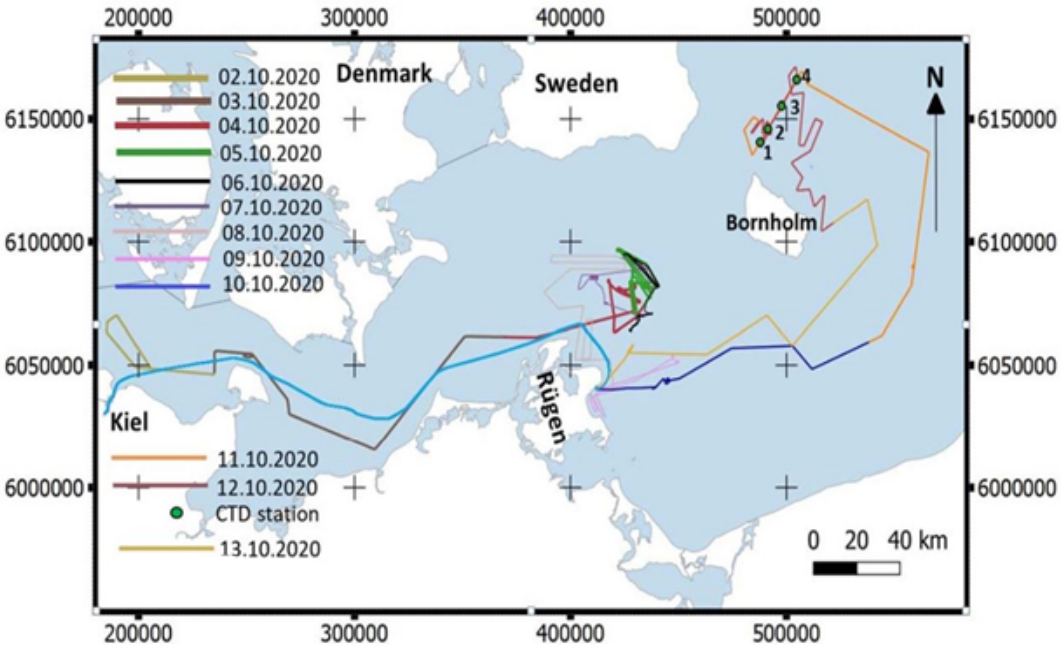


**Fig. 5.4:** Map of surveyed seismic profile in UTM value (from bay of Kiel to Bornholm basin).

Acquisition of seismic data ran through out, except for the 13th and 14th day of the cruise due to poor weather (Fig. 5.4). On day 13, to avoid storm on the Baltic Sea, the ship had to stay on the Sassnitz harbour. During this time, seismic brute stack for all profiles acquired were processed and uploaded into kingdom suite.

### 5.1.4 Data Example - Line Al546-GeoB-108 Bornholm Basin

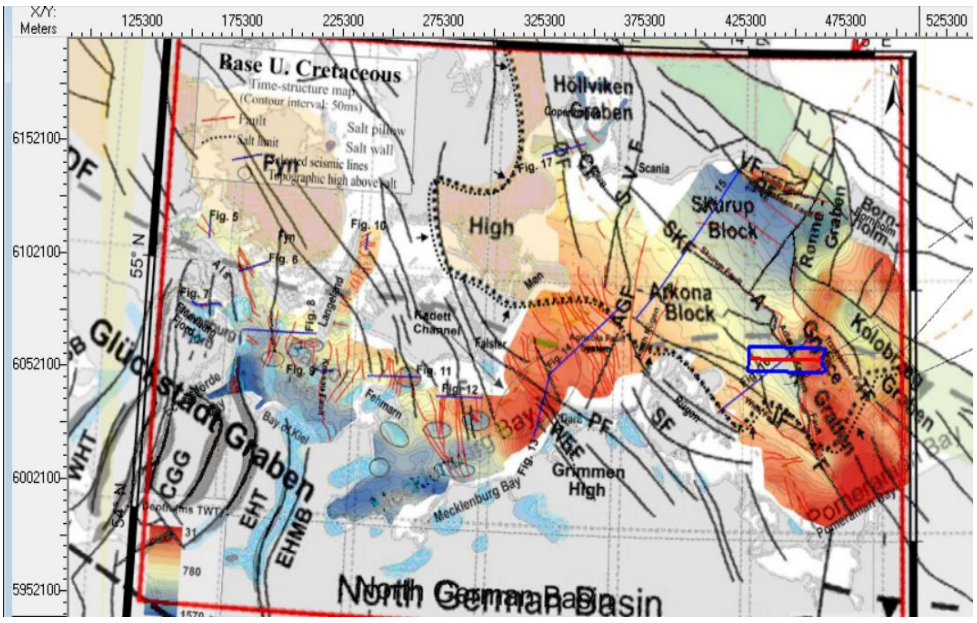


**Fig. 5.5:** Tectonic map of the Central European Basin System showing line Al546- GeoB-108. (modified after M. Al Hseinat and C. Hübscher, 2017).

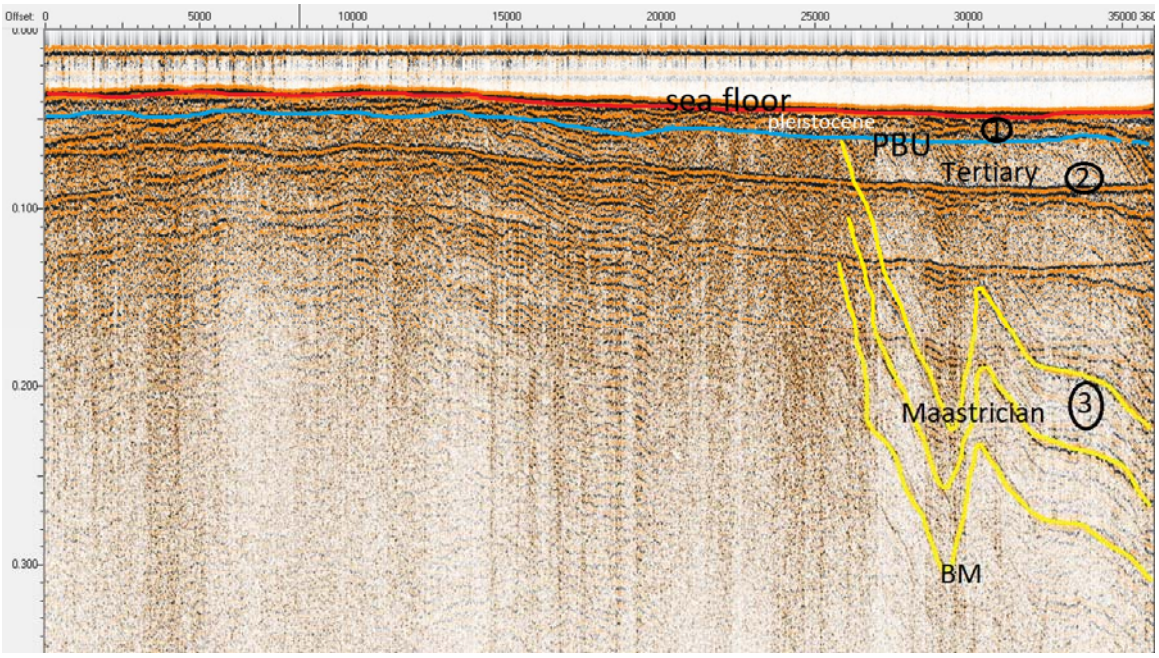


**Fig. 5.6:** Line Al546-GeoB-108 Bornholm basin. **BPU-**Base Pleisocene uncomformity, **BM-** Base Maastrician. Location is shown in Fig. 5.5 in relation to regional tectonics.

The seismic profile (Fig. 5.6) can be divided into 3 sections base on the characteristic of the reflectors. The first section consists of a horizon of relatively uniform thickness with parallel internal reflectors, the second section consist of both parallel and undulating reflectors with most of them top lapping at the base of the first horizon and the third section is dominated by strongly folded reflectors.

The Upper Cretaceous units represented here by the Pleistocene, Tertiary and the Maastrician units overly the base upper cretaceous horizon and is at the top bounded by the base of the Tertiary horizon northwest of the North German Basin and by the BPU reflection northeast of it. The unit consists mainly of chalk sediments deposited during shallow marine becoming open marine conditions and several parallel internal reflections can, however, be seen within this unit (Al Hseinat, M. And Hübscher, C., 2017).

The Tertiary unit overlies the BT horizon and extends upwards to the BPU reflection. The unit consists mainly of brackish marine clay-silt sediments (Scheck and Bayer, 1999). Two internal reflections are another characteristic of this succession.

The BPU represents an onlap or downlap surface which truncates the underlying Tertiary deposits. This erosional surface formed during Pleistocene times. The limited vertical resolution of the seismic data hampers the identification of Holocene strata in most regions except for the Little Belt (Al Hseinat, M. And Hübscher, C., 2017).

## 5.2 Sediment Echosounder

### 5.2.1 Background

The study of marine geology, morphology, wind farms and dredging operations in the offshore environment have led to an essential demand for precise seafloor maps. These applications require detailed information about seafloor composition and topography at the sediment surface and deeper layers. For this purpose, a more attractive technique has been developed with time, that classifies the seabed surfaces using single beam, multibeam and side scan sonars.

### 5.2.2 SES 2000 RV Alkor

The RV Alkor survey AL546 consist of a Parametric sub bottom profiler (SES 2000) for offshore applications among all the other equipment, designed by Innomar Technologie GmbH. The main aim of Sediment echosounder (SES) on board was to image the uppermost tens of meters of Holocene and glacial deposits, locally also shallow bedrock, at a high vertical and lateral resolution (cruise report).

The aim of the classical sub bottom profiler is to explore first layer of sediments below the seafloor reaching thickness of several tens of meters using a single frequency. Sediment structure is directly observed by measuring the elapsed time of the received reflections of the acoustic energy when it encounters boundaries of different sediment layers. Parametric acoustics perform well in a range of functions: they provide excellent penetration of the seabed and give good resolution even at low frequencies, and with higher frequencies they provide pinpoint accuracy regarding the depth of the water.

### 5.2.3 Equipment

In entirety the equipment consisted of a transducer and a main unit (with amplifiers, transmitters, and receivers, along with a chosen extension unit for the medium model, Fig. 5.7). Furthermore, a designated PC is required to effectively run the system software.

**Fig 5.7:** Equipment for SES 2000 medium - main unit (left), tranducer (right)

### 5.2.4 Nonlinear SBP

The parametric acoustical effect is used in the nonlinear parametric SBP since it is capable of transmitting 2 different high frequency signals simultaneously. The resulting interaction creates a new different low frequency signal. This resultant different and new frequency signal is distinguishable by short signal length, restricted beam width, and large bandwidth. It further makes it possible to get high levels of penetration and high resolution (with both vertical and horizontal directions) as well as to get narrow sound beams particularly at low frequencies

### 5.2.5 Working Principles

The SBP operations can be understood on simple principles of acoustics (Fig. 5.8). A set frequency is used to transmit sound pulses to the sea floor and wherever it encounters sea floor, boulders, or a sediment layer it reflects and echoes. These echoed signals then undergo a conversion through the transducers from acoustic to electrical signals. The converted electrical signals are then used for calculating an echo print, which across sailed tracks can reveal a sub-bottom structure. Depending on the specific sound speeds assumed, travel time can be calculated to reveal exact distance.

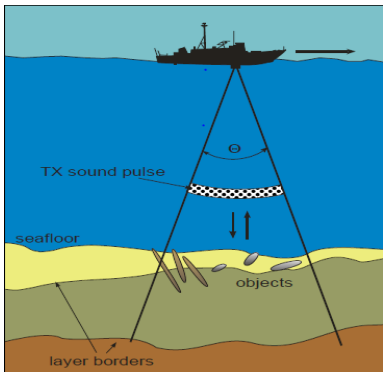


**Fig. 5.8**: Principle of sediment echosounder.

### 5.2.6 Limitations

The mechanism is simple at first glance, but various variables can disturb the quality and accuracy of the data. Some aspects are environmental while others are more technical limitations and flaws. The returning pulse strength is affected by signal attenuation, layer roughness and reflection coefficient.

The resolution is also dependent on the following factors:

- The sounded area size of the sea floor also known as the sound source footprint. The echo print that is retrieved (its horizontal resolution) depends on the footprint size hence for higher resolution a small footprint size should be opted.
- Similarly, the vertical resolution is controlled by the pulse length. In order to achieve better vertical resolution particularly in shallow water; shorter pulses and larger frequency bandwidths should be adopted.
- In order to lessen the sound to noise ratio pulse repetition ping/rate are important. They also contribute in identification of objects and features, the more times an object is hit the better signal reading it can provide.
- SBP are used for taking pictures of embedded objects in the sea floor therefore it is necessary for the frequencies to be able to penetrate the sea floor. Any sub-bottom profiling frequencies used need to be optimal for penetration as frequency is directly linked with depth of penetration hence low frequency pulses are best.
- Compensation carried out for ship movements (pitch, roll, and heave) will also affect the end data but is a necessary step to take.

Beam steering (especially at seabed slopes) is an effective technique to redirect the sound beam transmission to make it perpendicular to the seafloor as this ensures excellent penetration, sound to noise ratio and overall resolution. This process can be carried out on board ALKOR.

### 5.2.7 SES System Setup and Installation

The system installation is done in the following steps: the transducer should be secured and fixed properly and kept at a calculated distance from the ship's noise source. It should be well underwater before the system is turned on, with the computer (with the installed software) and main unit kept in a dry area away from moisture. It is worthwhile to note that if receiver and transducer are kept in the same location, horizontal positioning of objects and features will be more accurate and precise. If they are kept in different locations, reflected signals would need to be picked up by a hydrophone array at consideration distance from the source. Initial configurations are used to set up and connect the computer with software installed and the data can be viewed on the screen in the process of recording. The volume of data is generated directly from the equipment.

### 5.2.8 DATA Recording RV Alkor AL546

The SES survey along with other equipment was carried out to acquire geophysical data on transit, to complement long profiles between Kiel Bay, Rugen, Arkona Basin and Bornholm. Mostly Quaternary geology within the uppermost tens of meters into the subseafloor was imaged. The transducer settings were mainly the primary frequency of 100 kHz and 105/110/115 kHz. The secondary frequency that was produced was 5/10/15 kHz.

In the Leg of the expedition the SES was in constant data recording mode, halting only at the end of previous lines and when new lines began. As the track was being recorded it was essential to calibrate the software as required (depending on the depth of water). This was done to get as thorough as possible a recording of the seafloor and the SESWIN. A line recording is set by hitting stop key on the software once confirmation is received from the vessel bridge that the planned track has ended. The subsequent procedure is to wait for the ship to enter the change curve and when the center is reached a new profile is commenced on SESWIN after the record key is pressed as soon as the profile name is changed. Raw data is always visible on SESWIN during the process of recording which aids in the selection of appropriate recording ranges The lines preview the recorded data within ship protocol, furthermore all-important aspects such as time, location and depth are also provided.

A custom-made software called ps32segy was used for processing and interpretation of all the final data output (saved in ses format). The Kingdom software was deemed inadequate for data interpretation in this case so ps32segy created by Dr. Hanno Keil of Universitat Bremen was used. The conversion was however done after the selection of certain channel criteria such as difference frequency options and the final data was converted from .ses to .segy and saved, with the latter being a more suitable data format especially for Kingdom software. The final data sets were individually entered into Kingdom software for advanced interpretation.

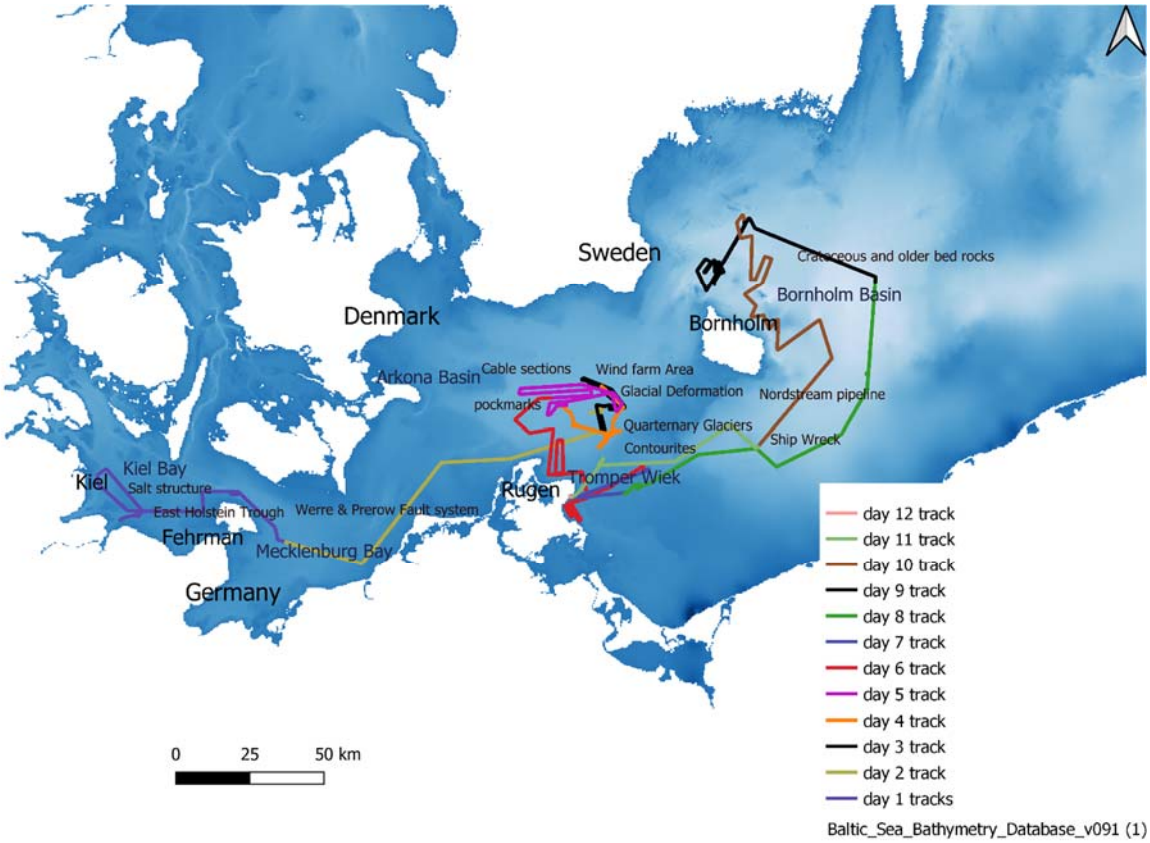


**Fig 5.9:** Tracks of RV Alkor survey AL546

### 5.2.9 Onboard Data Examples

Since SES was working throughout the survey some examples from RV Alkor survey 2020 are given below which show how the output data appears and how it can be interpreted further. The base map (Fig. 5.10) shows the SES survey carried out to trace power cable location within sea floor and upper tens of meters of sediments


**Fig. 5.10:** Bathymetric map of SES survey for power cables

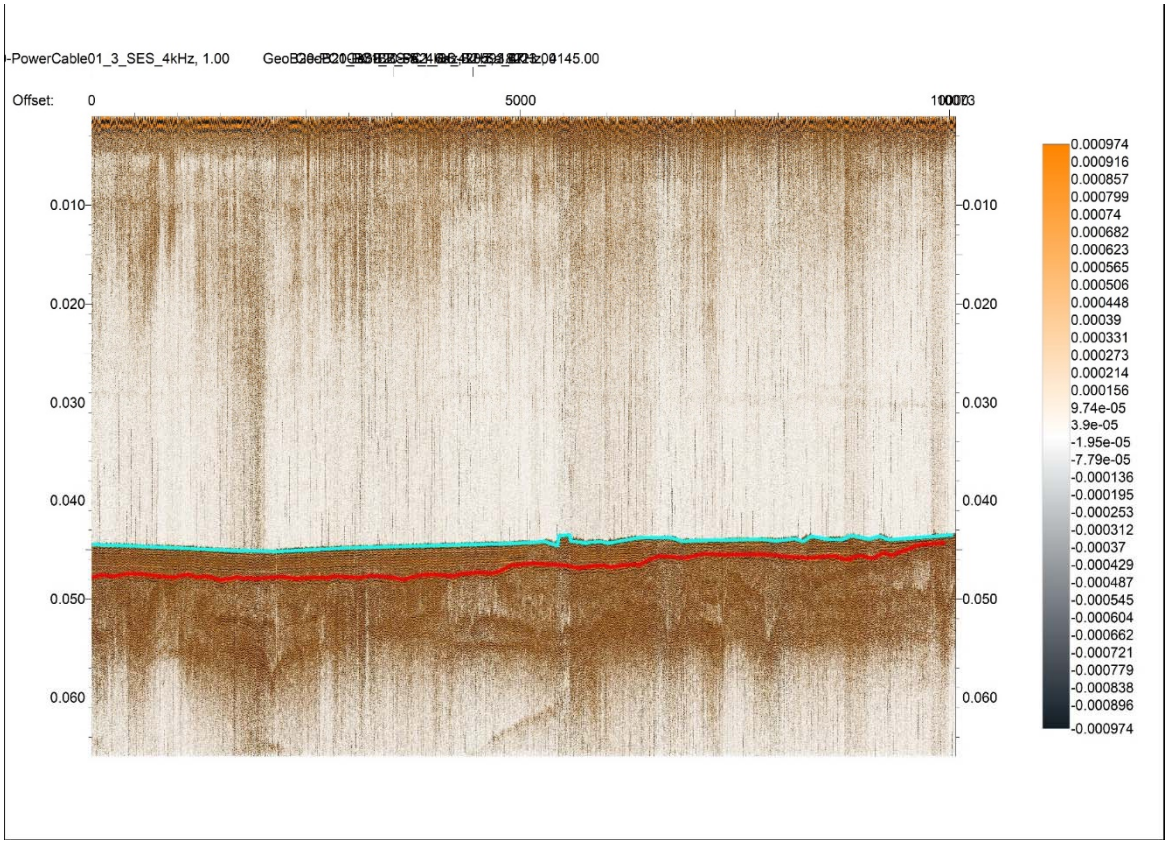


**Fig. 5.11:** Profile GEO B 20_POWERCABLE 1_2 SES with 4khz frequency, horizon 1 (cyan) showing sea floor and second horizon (red) marks the Holocene

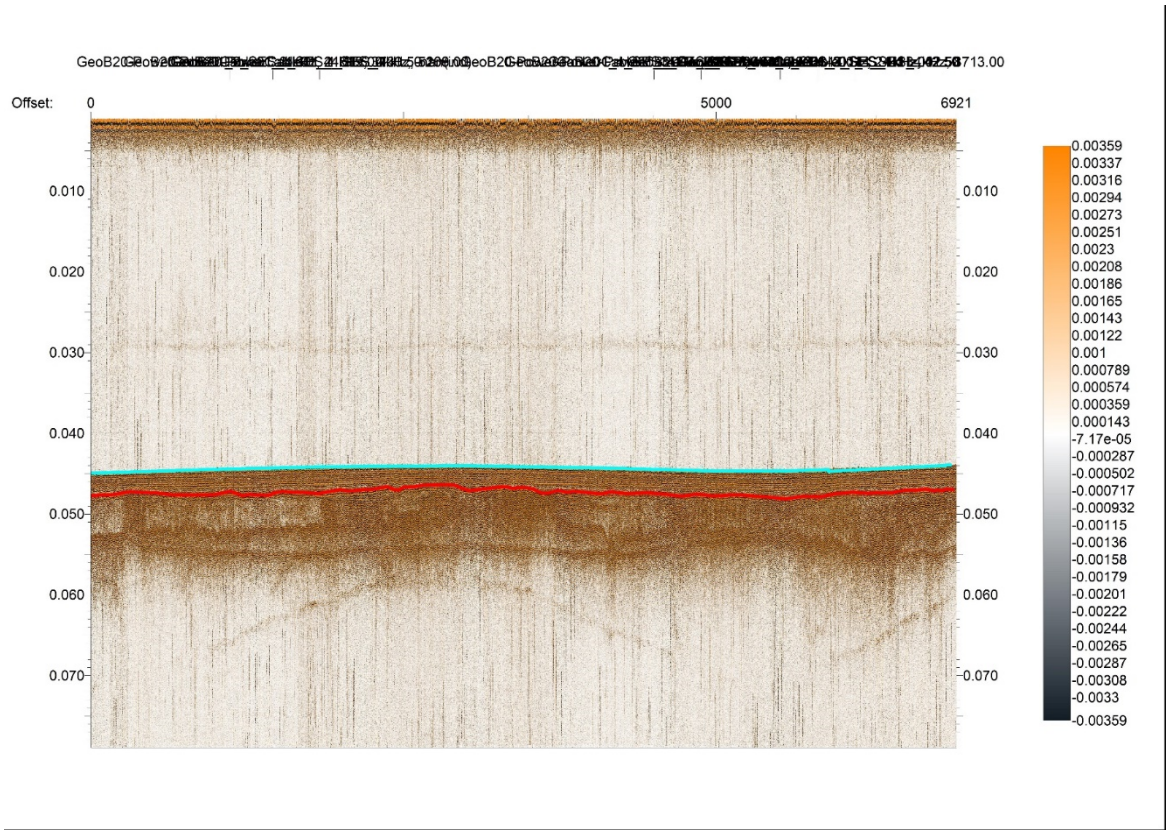


**Fig. 5.12:** Profile GEO B 20_POWERCABLE 1_BS_B2_6a with 4khz frequency horizon 1 (cyan) showing sea floor and second horizon (red) marks the Holocene.

## 5.3 Multibeam Echo Sounding Bathymetry

During the Alkor cruise AL546 a Norbit iWBMSe Multibeam sonar system operating at 400 kHz was used. The Norbit Multibeam Echosounder (MBES) is moonpool mounted and used through the vessels moonpool. The MBES location in relation its corresponding GPS receiver was poisoned 3 meters towards the aft of the ship, 4 meters on the port side, approximately 40cm below the ship, 14.8 meters below the GPS receiver. The position of the MBES moonpool on board Alkor is midship, at 19.25 meters from the aft, 1.64 meters to the port side. During the Alkor cruise AL546 the MBES was used for both bathymetry and backscatter acquisition. The MBES system is useful in imaging shallow water seafloor morphology and surveying manmade objects such as wrecks and pipelines. MBES Backscatter is considered separately in this report.

### 5.3.1 System Overview and Principles of Multibeam Echo Sounding Bathymetry

Multibeam Echo Sounding, MBES, systems have been developed for high-resolution bathymetry measurements and are today widely used in characterising seafloor morphology and bathymetry for a range of purposes from object detection, such as pipelines or wrecks, to morphology studies of for example mass wasting events, and ripple or sand wave field (Jakobson et al., 2016). Multibeam systems provide depth and backscatter information for a full swath of the seafloor across the vessel track, using up to 512 beams with the Norbit iWBMSe (Norbit, n.d.), instead of single depth measurement bellow the vessel using a single beam echo sounding system. From the MBES a signal is sent towards the seafloor across the vessel track from a transmitter and received from multiple locations using receivers that listen to the signal along the ships track. This results in several readings of the depth at discrete spots at the seafloor (Jakobsson et al., 2016). Commonly MBES surveys are run in a pre-planned grid, to allow for 100% seafloor coverage in the surveyed area. Important in MBES surveying is swath coverage, meaning the zone surveyed in a single sweep. In planning the water depths must be taken into consideration and lines spaced so that each survey line runs parallel to each other, without leaving a gap between the swaths at the seafloor. Generally, a good linespacing is 3 to 4 times the water depth of the survey area (IHO, 2008).

For multibeam surveying multiple standards exist, such as the S-44 by the International Hydrographic Organization, IHO (IHO, 2008). These outline well the different parts often included in multibeam surveys, and will therefore only be considered in brief. There are multiple factors that need to be taken into consideration during a successful MBES surveys.

The Norbit iWBMSe has inbuilt transducers and inertial navigation system to allow for real-time motion correction and positioning using GPS (Norbit, n.d.). Using high quality positioning and movement correction improves data quality and minimises possible errors in overlap of data, so that features on the seafloor occur at the same location at each survey run. Movement compensation calculates the position of the MBES transducers at any given time to compensate for vessel (and resulting transducer) movements such as roll and pitch. This is required to maintain constant depths in the data during MBES surveying (Reson, 2006). Artefacts arising from incorrect or missing movement corrections include for example wobbly appearance of the outer beams and miss fitting between subsequent survey lines. Especially calibrating pole mounted MBES systems prior to use is important to avoid artefacts due to bad calibration or motion compensation

(Jakobsson et al., 2016).

Ping rate is the frequency at which signals are sent from the transducer. A faster ping rate results in more depth readings in total. The Norbit iWBMSe has an adaptive ping rate up to 60 Hz and adjusts automatically the ping rate to suit mainly the depth of the survey area (Norbit, n.d.). If the ping rate is too low, or vessel speed is too high, the density of the measurements in the movement direction of the vessel become more spars, and detail of the seafloor morphology is lost. Commonly high frequency systems can produce shorter signal pulses, that result in better vertical resolution (Jakobson et al., 2016).

The Frequency used in the Norbit iWBMSe during the Alkor cruise was 400 kHz. Higher frequencies have better vertical and horizontal resolutions resulting in for example better object identification. High resolution systems, such as the MBES do not penetrate the subseafloor in as large extent as e.g. the Innomar SES 200 also deployed during this Alkor cruise, and are therefore used in bathymetry and seafloor morphology studies not requiring seafloor penetration (Innomar, 2009). Higher frequencies attenuate faster in the water column, resulting in loss of signal at large depths. This is not a considerable problem in the Baltic Sea with generally shallow waters (Jones, 1999). The high resolution offered by the MBES system in both vertical and horizontal directions are dependent on the physical parameters commonly referred to as the Fresnel zone and Rayleigh Criterion, that both are frequency dependent (Jakobsson et al., 2016). The simplified relationship between frequency, depth and resolution are shown below.

$R_f \approx \sqrt{\frac{H\lambda}{2}}$, $H$ = water depth, $\lambda$= wavelength, $R_f$ = radius of Fresnel Zone / radius of the smallest theoretical zone that can be resolved

$R_v \approx \frac{\lambda}{4}$, $R_v$ = theoretical vertical resolution according to the Rayleigh Criterion, $\lambda$= wavelength

$\lambda = v/f$, $\lambda$ = wavelength, $v$ = velocity, $f$ =frequency

For MBES sound velocity profiling (SVP) is important for high quality data. The MBESechosounder sends beams in multiple different angels towards the seafloor, and therefore refraction in the water column is taken into consideration when surveying. If sound velocity information is completely wrong, it will cause artefacts in the MBES data in form false depth information at the far sides of the beam. Additionally, the overall depth uncertainty decreases with poor sound velocity profiling (Jones, 1999).

### 5.3.2 Usage and Data Example

During the Alkor AL546 cruise the Norbit iWBMSe was most of the time in use. A comprehensive list of survey lines is found in chapter 7. The MBES data, both bathymetry and backscatter, are collected together with sounding and seismic data from other measurements apparatus. During the cruise the MBES system was used on multiple targets. Surveyed objects and areas included ripple fields, cable corridors and existing cables in the vicinity of the wind parks Wikinger and Arkona Südost in the Arkona Basin, and pockmark surveys. The MBES system was also used for bathymetry and backscatter characterisation of the wreck of passenger ship Jan Heweliusz (Fig. 5.13). Additionally, surveys on the Nord Stream pipeline were conducted using both MBES and sediment echosounder to analyse the size and possible burial depth of the pipeline along with providing data on its precis location. In Figure 5.13 an example of the MBES bathymetry data on the Jan Heweliusz is shown.

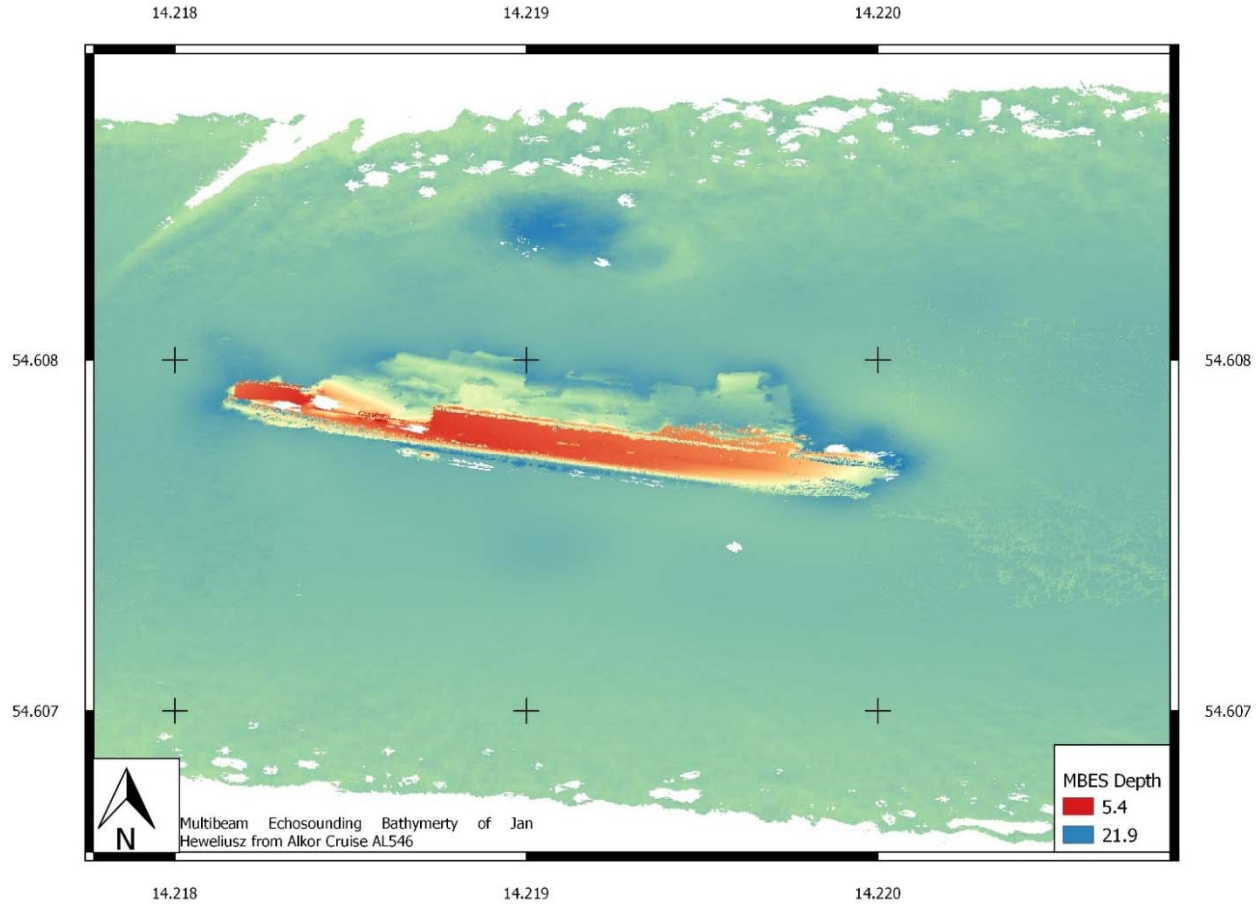


**Fig. 5.13:** The shipwreck of Jan Heweliusz as seen in the Multibeam Echo sounding bathymetry data from the Alkor cruise AL546. Coordinates are given in WGS84.

## 5.4 Multibeam Backscatter

Multibeam backscatter data provides information on the 'hardness' of the sea floor and is used to differentiate between different types of sea floor, such as hard rock or soft sediment. Backscatter data can be used as a proxy to understand the characteristics of the sea floor; including the sea floor hardness and surficial sediment characteristics. Backscatter data can also provide information on the sediment grain-size and sea floor roughness.

Backscatter data is used for a range of purposes such as:

- environmental management, including establishing baseline data to support environmental monitoring by providing the environmental characteristics of the sea floor (for example sea floor hardness, surficial sediment characteristics, and benthic habitat characteristics).
- assessment of environmental considerations for marine geology resource management including the identification of geohazards, such as underwater landslides
- environmental modelling (for example mapping habitat types at continuous scales)
- monitoring of anthropogenic changes in the sea floor (for example monitoring pipeline locations)
- safety navigation (for example monitoring and mapping of rocky areas or areas of hard ground)

Multibeam echo sounders (MBES) were used in the cruise to survey the sand ripple fields occurring in the cruise area. The MBES survey of the ship wreck location (in cruise area) was aimed at imaging the ship wreck lying on the seafloor in terms of its bathymetric and backscatter characteristics. MBES is one of the systems used to focus on surveying an underwater gas pipeline, the Nordstream pipeline that carries gas from Russia to Germany. The survey should reveal the size, height and/or burial depth, and provide data for its precise location.

### 5.4.1 Principles of Multibeam Backscatter Theory

At that moment when the transmitted acoustic pulse impinges the seafloor, it is scattered in all directions. Only a part of the incident wave is reflected in the specular direction. The part that will be scattered back towards the transducer is called backscatter (Fig. 5.14). In contrast to plane wave reflection, backscattering means that the acoustic wave is reradiated from the obstacle acting like a new source (Lurton, 2002).

Multibeam sonar systems use backscattered echoes for measurements. Other returns of the transmitted pulse towards the sonar system that are not originating from the desired target (backscattering from fish, suspended particles, plankton) is called reverberation and not included in the term backscatter (Lurton, 2002).

The seabed is usually not a plane surface. However, it can be assembled from a locally plane surface with a micro scale roughness. The effect of the micro roughness on the sonar wave depends on the roughness characteristics, the angle of incidence and the acoustic frequency (Lurton, 2002). The roughness of the seabed is the reason why the incident wave is scattered in all directions. The

ratio of scattered and specular components also depends on the surface roughness (ratio of relief amplitude and the sonar wave length) (Lurton, 2002).

The backscatter strength of the seafloor (target strength) is defined as the ratio between the intensity of the acoustic pulse scattered back by the seafloor and the incident intensity. It represents the relative amount of energy sent back by the target. It depends on the physical nature of the seabed, its structure (roughness) and the characteristics of the acoustic pulse (incidence angle, frequency). Because of the large range of that ratio it is logarithmized to obtain the unit decibel (dB).

The intensity of the echo received at the transducer depends on the transmitted source level, the transmission loss (absorption in the water column and geometrical spreading), and the target strength.

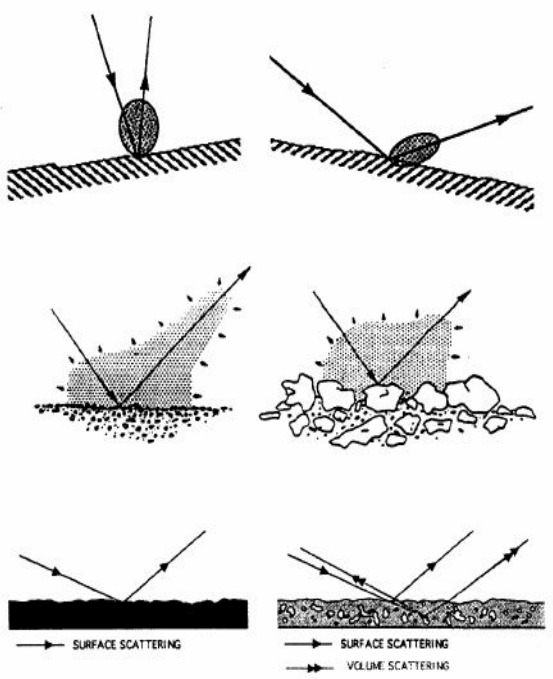


**Fig. 5.14:** Backscattering from the seafloor is influenced by three factors (from top to bottom): local geometry of insonification, roughness of the seafloor at scales comparable to the sonar's wavelength, intrinsic properties of the seafloor (e.g. rocks vs. sediments) (from Blondel and Murton, 1997)

For small targets like fish, the target strength refers to the object. Because the entire seafloor cannot be insonified by the echo pulse at once, the backscatter strength is therefore referring to a unit scattering element (dB re 1m2) (Lurton, 2002).

Acoustic frequencies that are used with sonar mapping systems lie in the range of tens to hundreds of kHz. Two main sources of backscattering act at these frequencies: interface and volume scattering (Lurton, 2002).

The interface scattering is basically due to the surface relief. Volume scattering occurs due to heterogeneities in the sediment (e.g. buried stones, shells, organisms, gas bubbles) and affects the part of the acoustic signal that penetrates the seabed (Fig. 5.14). It becomes dominant with increasing incidence angle and depends on the transmission and absorption in the sediment and on the volume backscattering strength of the sediment components. The lower the frequency, the more

acoustic energy penetrates the sediment (Urban, 2002).

The multibeam echosounder (MBES) used during the cruise has a frequency of 400 kHz and images in shallow water the seafloor morphology and measures roughness/lithology/grain size, pockmarks or man-made objects (cables, foundations, wrecks) through its backscatter characteristics.

Statistical geometrical models are appropriate to describe the interface backscattering (Lurton, 2002). They also account for the reflection coefficient of the interface. The interface roughness of the seabed can be described by the Rayleigh parameter which represents the ratio between the mean amplitude of the relief and the acoustic wavelength. It also considers the angle of incidence (Fig. 5.15). However, it applies to coherent reflection instead of scattering and is not relevant when modelling echoes directly backscattered from the seabed (Lurton, 2002).

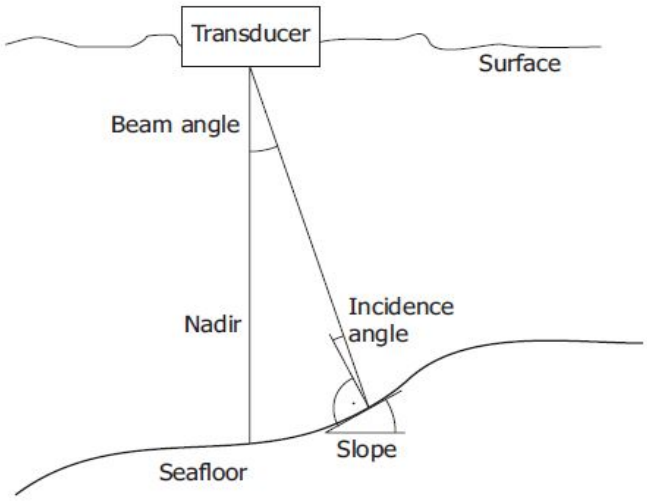


**Fig. 5.15:** Sketch of basic elements acting in the multibeam – seafloor regime.

The seabed structures and characteristics that can be analysed depend on the acoustic frequency used. Surface roughness at the seafloor (that is of interest at sonar frequencies) depends on geology and covers a scale range between millimetres and a few metres (Lurton, 2002)

A combination of different scales of micro-roughness can coexist. The seabed may show for example sand ripples having centimetre scale roughness overlaying large-scale sand dunes which differently affect the acoustic pulse. Rocky and sedimentary seabed is in general referred to as rough and smooth surfaces, respectively.

### 5.4.2 Methods for Collecting Backscatter Data

Multibeam bathymetry and multibeam backscatter data are collected at the same time using a multibeam echosounder mounted on a survey vessel. While bathymetry measures ocean depth, backscatter can be used to measure sea floor hardness.

During data collection, multibeam echosounders send out multiple sound waves that bounce off the sea floor and return to the ship. These sound waves are emitted as acoustic pulses. From each pulse, a co-located bathymetry and backscatter measurement is collected. Each acoustic pulse propagates from the vessel in a line of beams from left to right, fanning out under the vessel; this is known as the beam pattern. The beam pattern is wide across-track, which means it covers the area immediately under the vessel, and on either side of the vessel, and narrow along-track, which means it does not cover the area in front or behind the vessel (Fig. 5.17).

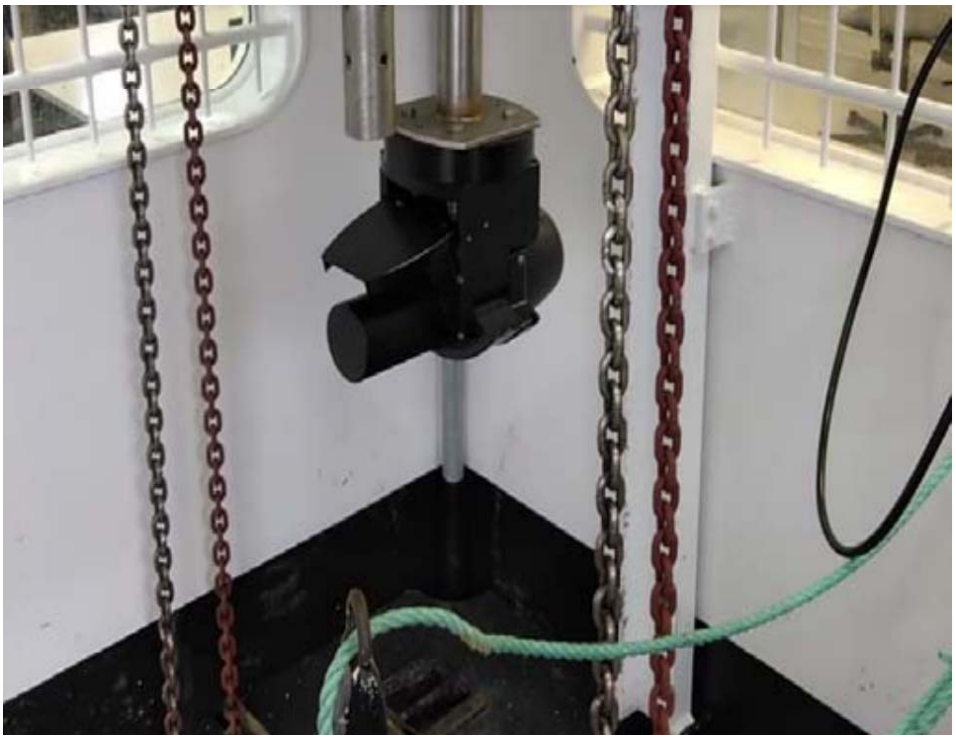

**Fig. 5.16:** Multibeam echosounder hangin above the moonpool.

The delay between sending the signal from the transmit arrays and receiving the acoustic returns provides a measurement of ocean depth, or bathymetry data while the strength of the return signal provides an indication of how hard the sea floor is, or backscatter data.

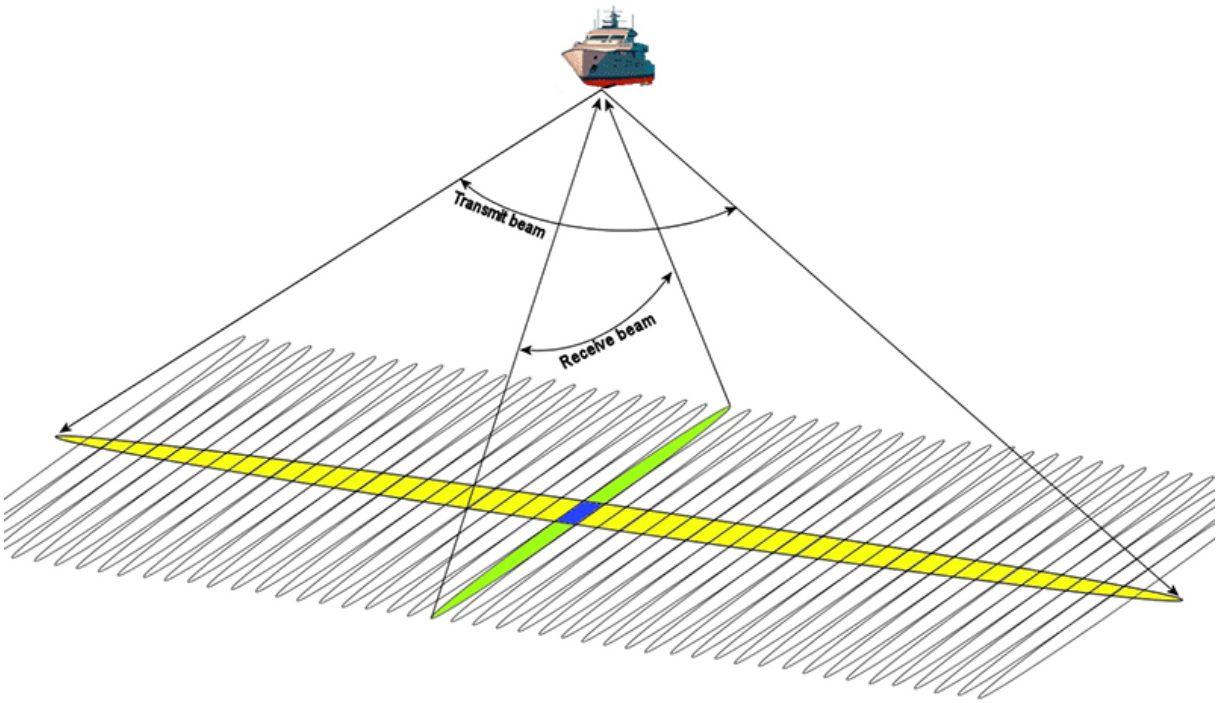


**Fig. 5.17:** Example of multibeam backscatter data collection where yellow represents the transmit beam, green is an example of one of the received beams and blue is a single footprint formed by the intersection of the two (2017 Image from AML-Oceanographic).

From the cruise decks plan (see App. 1) AL546 on the research vessel, the locations/points of interest for instruments used are as follows:

Multibeam echosounder: -19.25(x), -1.64(y), -0.04(z)
GPS Multibeam: -23.07(x), -5.56(y), 15.26(z)

These coordinate systems are in accordance with Wingeoapp's specifications:

- Starboard(+), Port(-), Stern(+), Bow(-)
- y-axis(across track); x-axis(along track); z-axis(vessel height)

MBES data acquisition in the Arkona Basin mainly targeted the backscatter signature from two buried cable sections of the land connection to two major Windparks (Wikinger, Arkona Südost). Three parallel passes provided full MBES coverage of the cable corridor.

Detailed MBES data acquisition was carried out to study the backscatter received in two known pockmark locations to determine/confirm the nature and size of pockmarks in each location (profile map in Fig. 5.18). Further very shallow subsurface gas patches were surveyed to potentially identify more pockmarks in multibeam data from depth and backscatter measurements. Water column was also recorded to study potential bubble release from pockmarks.

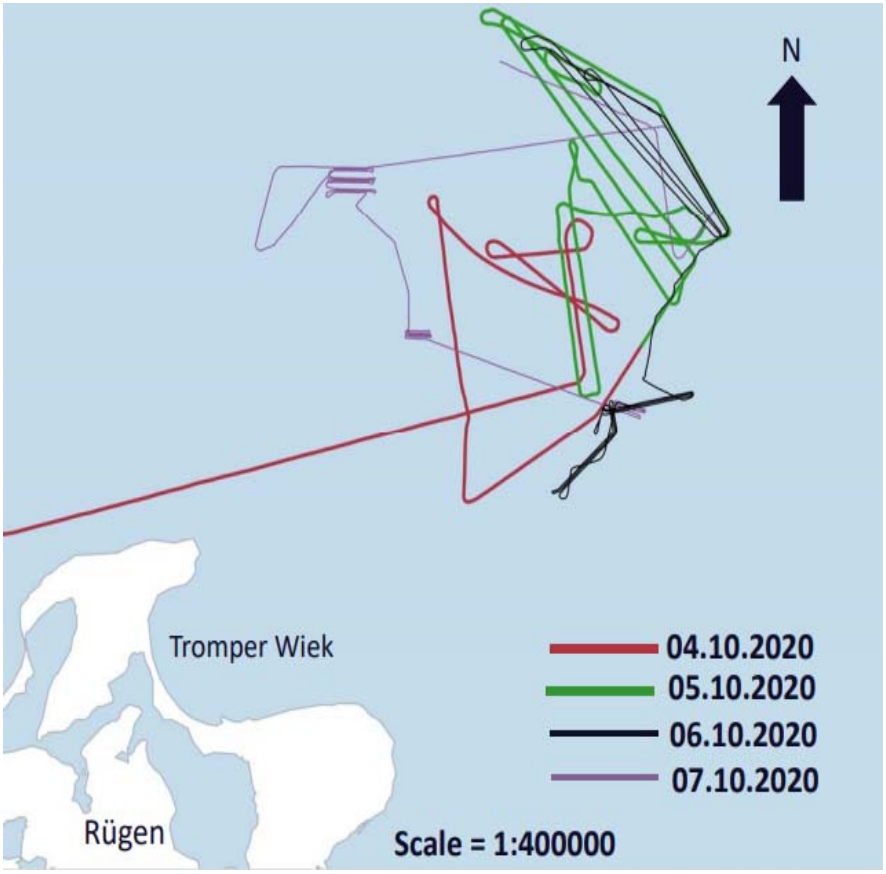


**Fig. 5.18:** Map of measured Profiles: GeoB20-BS-12; GeoB20-BS-B2; GeoB20-BS-6; GeoB20-BS-3

### 5.4.3 Processing of Backscatter Data

The proportion of acoustic energy reflected back from the seabed is determined by the impedance contrast, sometimes referred to as 'hardness' and apparent surface roughness scale (i.e. roughness relative to the acoustic wavelength). In general, backscatter intensity increases with surface roughness or hardness.

The surface scattering coefficient is a dimensionless quantity that accounts for the intensity (power) ratio of the incident and scattered waves determined per unit area at a reference distance of 1 m. When expressed in decibels (dB), this quantity is commonly called the backscatter strength (BS).

Backscatter processing involves radiometric and geometric corrections. The processing steps include the removal of the system transmission loss; removal of the sonar system's specific angular dependence correction model; calculation of the angle of incidence; correction of the beam pattern; calculation of the angular backscatter response within a predefined window; and removal of the angular dependence and restoration to the backscatter strength at a chosen reference angle. Two processed backscatter datasets produced are a backscatter mosaic and a set of angular backscatter response curves.

As the transmitted acoustic pulse sweeps the seafloor from the nadir towards outer beams, the size of the insonified area varies due to the directivity pattern. In the nadir area the footprint of the beams are insonified completely by the acoustic pulse while in the outer parts of the swath the

pulse slice travels through the footprint (Fig. 5.19). This situation is included during processing to yield backscattering strength.

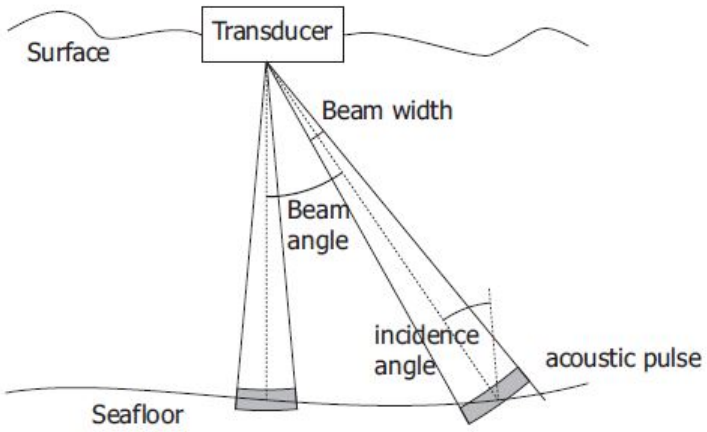


**Fig. 5.19:** Geometry of the seafloor insonification by vertical beams, limited by the directivity and oblique beams, limited by the pulse length

### 5.4.4 Multibeam Backscatter Analysis

Detailed and accurate bathymetry is mandatory to calculate backscatter strength. Overlapping swaths of adjacent survey lines are a precondition to achieve accurate models of the seafloor. Therefore, the bathymetric data set is not completely available until the cruise has been completed. The calculation of the seafloor backscatter strength in this cruise was realized in post-processing. Furthermore, the recorded depth data are not sufficiently processed during real time data acquisition.

The slope of the seafloor directly affects the computed angle of incidence of the transmitted beam. The shape of the angular backscatter function and its spatial variation gives indication about the geological facies. The reason to relate backscatter of the seafloor to the type of seabed (mud, silt, sand, boulders, and rock) originates from the observation that rocky seabed shows greater backscatter than muddy areas. However, the particle size of the sediment can only act as indirect indicator for scattering (Urick, 1983). The roughness of the seabed represents the main factor of the backscattering characteristic. Due to the relationship between surface roughness and seabed type, the roughness serves as proxy for the geological facies when using multibeam backscatter data. Research is still ongoing regarding the connection between angular backscatter strength and seabed factors, i.e. incidence angle, local slope, micro roughness and sediment properties (composition, density, relative importance of volume vs. surface scattering).

The Lambert law is the simplest model that describes the angular backscatter as linear function of the square cosine of the incidence angle. It only works in simple regimes (smooth surfaces and large scale undulations) and does not resemble the complex reality (Blondel and Murton, 1997). Other models are based on the interference of scattered elementary waves composing the echo acoustic field.

The Helmholtz-Kirchhoff theory describes the seafloor using the root-mean-square roughness of the vertical dimension and the correlation radius in horizontal dimension (de Moustier, 1986).

The model developed by Jackson et al. (1986) relates the angular backscatter data to a series of parameters describing the sediment (surface roughness, seabed/ seawater sound velocity and density ratio and ratio of volume scattering versus sediment attenuation coefficient).

# 6 Station List AL546

## 6.1 Station List

| Station No. | | Date | Gear | Time | Latitude | Longitude | Water Depth | Remarks/Recovery |
|---|---|---|---|---|---|---|---|---|
| AL546_ | GeoB20- | 2020 | | [UTC] | [°N] | [°E] | [m] | |
| 2-1 | CTD 1 | 12.10. | CTD | 05:07 | 55° 24.677 | 14° 48.522 | 68,9 | CTD Location 1 (Water depth: 68.9m; Winch velocity: 0.1 mls) |
| 3-1 | CTD 2 | 12.10. | CTD | 06:08 | 55° 27.564 | 14° 51.896 | 74,8 | CTD Location 2 (Water depth: 74.8m; Winch velocity: 0.1 mls) |
| 4-1 | CTD3 | 12.10. | CTD | 07:18 | 55° 32.597 | 14° 57.880 | 79,5 | CTD Location 3 (Water depth: 79.5m; Winch velocity: 0.1 mls) |
| 5-1 | CTD4 | 12.10. | CTD | 08:26 | 55° 38.225 | 15° 4.597 | 75,0 | CTD Location 4 (Water depth: 75m; Winch velocity: 0.1 mls) |

## 6.2 Seismic/Acoustic Profile List

| Profile No. | | Date | Gear | Time | Latitude | Longitude | Water Depth | Remarks/Recovery |
|---|---|---|---|---|---|---|---|---|
| AL546_ | [GEOB20-] | 2020 | | [UTC] | [°N] | [°E] | [m] | |
| 1-2 | 001-Pre | 02.10. | Micro-GI Multibeam | 13:40 | 54° 30.242 | 10° 26.778 | 10,0 | |
| 1-2 | 001 | 02.10. | Micro-GI Multibeam | 13:47 | 54° 30.621 | 10° 26.261 | 10,0 | |
| 1-2 | 002 | 02.10. | Micro-GI Multibeam | 16:31 | 54° 40.723 | 10° 10.625 | 22,0 | |
| 1-2 | 003 | 02.10. | Micro-GI Multibeam | 17:03 | 54° 38.984 | 10° 7.346 | 24,3 | |
| 1-2 | 004 | 02.10. | Micro-GI Multibeam SES | 17:30 | 54° 36.940 | 10° 7.690 | 23,8 | |
| 1-2 | 005 | 02.10. | Micro-GI Multibeam SES | 19:45 | 54° 29.954 | 10° 21.378 | 18,5 | |
| 1-2 | 006 | 03.10. | Micro-GI Multibeam SES | 00:06 | 54° 30.177 | 10° 54.416 | 12,2 | |
| 1-2 | 007 | 03.10. | Micro-GI Multibeam SES | 01:08 | 54° 34.778 | 10° 54.985 | 15,8 | Shooting interrupted during profile, temporary deviation from track |
| 1-2 | 008 | 03.10. | Micro-GI Multibeam SES | 05:10 | 54° 34.506 | 11° 10.299 | 27,9 | |
| 1-2 | 009 | 03.10. | Micro-GI Multibeam SES | 08:26 | 54° 24.931 | 11° 26.344 | 4,4 | |
| 1-2 | 010 | 03.10. | Micro-GI Multibeam SES | 09:01 | 54° 22.04 | 11° 27.29' | 23,0 | |
| 1-2 | 011 | 03.10. | Micro-GI Multibeam SES Hydro | 14:19 | 54° 15.221 | 12° 4.678 | 12,3 | During the second half of profile 11 testing of the single hydrophone started. Recoring with 8-channel MaMuCS. During testing phase (~17:00-20:00) pressure changex several times. |
| 1-2 | 012 | 03.10. | Micro-GI Multibeam SES Hydro | 21:46 | 54° 40.693 | 12° 41.239 | 20,0 | |
| 1-2 | 013 | 04.10. | Micro-GI Multibeam SES Hydro | 01:46 | 54° 41.084 | 13° 12.356 | 23,0 | |
| 1-2 | 014 | 04.10. | Micro-GI Multibeam SES Hydro | 07:21 | 54° 47.737 | 13° 54.262 | 41,0 | |
| 1-2 | 015 | 04.10. | Micro-GI Multibeam SES Hydro | 08:43 | 54° 52.937 | 13° 54.549 | 44,7 | |
| 1-2 | 016 | 04.10. | Micro-GI Multibeam SES Hydro | 10:03 | 54° 52.267 | 13° 47.961 | 45,2 | Recording interrupted after Profile 16 to prepare Experiments with Mini GI Gun in True GI-Mode; Multibeam recording Switch off |
| 1-2 | 017-exp | 04.10. | Micro-GI SES Hydro | 12:05 | 54° 50.004 | 13° 54.756 | 43,8 | testing Micro-gi-gun source signature (see Source-signature recording Protokoll for detail) |
| 1-2 | 018 | 04.10. | Micro-GI Multibeam SES | 21:17 | 54° 45.927 | 13° 45.815 | 41,0 | end of testing different setups, back to normal 2d seismic acquisition; Geometrie set up changed, recording lenght 8-channel MaMuCS changed to 950 ms |
| 1-2 | 019 | 04.10. | Multibeam SES | 21:57 | 54° 42.860 | 13° 45.557 | 38,0 | |

| | | | | | | | | |
|---|---|---|---|---|---|---|---|---|
| 1-2 | 020 | 04.10. | Micro-GI Multibeam SES | 23:17 | 54° 45.936 | 13° 55.168 | 38,5 | |
| 1-2 | 021 | 05.10. | Micro-GI Multibeam SES | 00:45 | 54° 51.643 | 14° 2.2300 | 41,1 | |
| 1-2 | 022 | 05.10. | Micro-GI Multibeam SES | 03:38 | 55° 0.185 | 13° 48.080 | 46,1 | trigger problems, no communication to first bird |
| 1-2 | 023 | 05.10. | Micro-GI Multibeam SES | 06:08 | 54° 50.789 | 14° 1.379 | 40,5 | |
| 1-2 | 024 | 05.10. | Micro-GI Multibeam SES | 06:20 | 54° 50.296 | 14° 0.383 | 40,4 | time correction 1.11s |
| 1-2 | 025 | 05.10. | Micro-GI Multibeam SES | 08:37 | 54° 55.570 | 13° 53.482 | 45,9 | Recording lenght 8-channel MaMuCS changed to 200 ms during profile (saved in -25b) |
| 1-2 | 026 | 05.10. | Micro-GI Multibeam SES | 10:35 | 54° 46.871 | 13° 53.973 | 40,0 | Issues with micro-GI trigger, after profile end gun retrival, switch to GI-Gun |
| 1-2 | 027 | 05.10. | GI Multibeam SES | 12:04 | | | | Maintenance during profile thus no protocol entries, but raw data were recording with both MaMuCSs. Shot rate changed to 15000 ms |
| 1-2 | 028 | 05.10. | GI Multibeam SES | 13:13 | 54° 53.532 | 13° 54.156 | 45,0 | during profiles 28 and 29 depressor experiments using GI-Gun |
| 1-2 | 029 | 05.10. | Micro-GI GI Multibeam SES | | | | | |
| 1-2 | 030 | 05.10. | Micro-GI Multibeam SES | 18:47 | 54° 54.611 | 14° 2.847 | 44,0 | |
| 1-2 | 031 | 05.10. | Micro-GI Multibeam SES | 19:23 | 54° 57.620 | 13° 59.225 | 46,5 | |
| 1-2 | 032 | 05.10. | Micro-GI Multibeam SES | 21:07 | 54° 0.853 | 13° 46912 | 46,3 | |
| 1-2 | 033 | 06.10. | Micro-GI Multibeam SES | 01:24 | 54° 56.677 | 14° 0.442 | 45,8 | |
| 1-2 | 034 | 06.10. | Micro-GI Multibeam SES | 02:31 | 54° 52.738 | 14° 3.602 | 41,5 | During recording pressure drop; Micro-GI retrival at the end of profile, gun maintenance; then gun redeployment Micro-GI |
| 1-2 | 035 | 06.10. | Micro-GI Multibeam SES | 05:14 | 54° 59.89 | 13° 49.98 | 46,3 | |
| 1-2 | 036 | 06.10. | Micro-GI Multibeam SES | 07:41 | 54° 52.913 | 14° 0.463 | 41,0 | Micro-GI Generator issues; Generator is triggered with delay. During Profiles 36-38 tests with different pressures to solve delay issues. Gun retrevial at the end of profile 038 |
| 1-2 | 037 | 06.10. | Micro-GI Multibeam SES | 08:43 | 54° 57.228 | 13° 59.199 | 46,3 | |
| 1-2 | 038 | 06.10. | Micro-GI Multibeam SES | 09:13 | 54° 58.339 | 13° 55.251 | 46,7 | |
| 1-1 | PowerCable01 | 06.10. | Multibeam SES | 16:22 | 54° 46.795 | 14° 0.725 | | |
| 1-1 | PC1-BS-3B-6 | 06.10. | Multibeam SES | 18:59 | 54° 46.018 | 13° 56.005 | 38,3 | Beam steering of SES with 3 beam angles (-6, 0, 6) |
| 1-1 | PC1-BS-3B-12 | 06.10. | Multibeam SES | 23:00 | 54° 43.703 | 13° 53.374 | 36,9 | SES beam angles changed to -12.8, 0, 12.8 |
| 1-1 | PC1-BS-3B-9 | 06.10. | Multibeam SES | 23:21 | 54° 44.615 | 13° 55.893 | 37,2 | SES beam angles changed to -9.6, 0, 9.6 |
| 1-1 | PC1-BS-LF4-H | 06.10. | Multibeam SES | 23:48 | 54° 46.439 | 13° 56.782 | 38,2 | SES set to single frequency mode, 4 kHz |
| 1-1 | PC1-BS-2B-12 | 07.10. | Multibeam SES | 00:36 | 54° 46.438 | 13° 57.020 | 38,2 | SES set to beamsteering mode, beam angles set to -12.8, 12.8 |
| 1-1 | PC1-BS-2B-9 | 07.10. | Multibeam SES | 01:13 | 54° 46.487 | 13° 56.883 | 38,3 | SES beam angles changed to -9.6, 9.6 |
| 1-1 | PC1-BS-2B-6 | 07.10. | Multibeam SES | 01:56 | 54° 46.451 | 13° 56.927 | 38,3 | SES beam angles changed to -6, 6 |
| 1-1 | PC1-BS-2B-3 | 07.10. | Multibeam SES | 02:37 | | | | SES beam angles changed to -3, 3 |
| 1-1 | PC-Transit | 07.10. | Multibeam SES | 03:30 | 54° 45.96 | 13° 58.00 | 37,8 | |
| 1-1 | PM1-1 | 07.10. | Multibeam SES | 05:27 | 54° 48.68 | 13° 42.30 | 43,4 | |
| 1-1 | PM1-2 | 07.10. | Multibeam SES | | 54° 48:729 | 13° 41:066 | | |
| 1-1 | PM1-3 | 07.10. | Multibeam SES | 06:00 | 54° 48.823 | 13° 42.954 | 43,6 | |
| 1-1 | PM1-4 | 07.10. | Multibeam SES | 06:15 | 54° 48.818 | 13° 41.148 | 43,7 | |
| 1-1 | PM1-5 | 07.10. | Multibeam SES | 06:33 | 54° 48.975 | 13° 43.847 | 43,5 | |
| 1-1 | PM1-6 | 07.10. | Multibeam SES | 06:49 | 54° 48.952 | 13° 41.12 | 43,6 | |
| 1-1 | PM1-7 | 07.10. | Multibeam SES | 07:06 | 54° 48.804 | 13° 42.875 | 43,5 | |
| 1-1 | PM-Tranist | 07.10. | | 07:24 | 54° 49.189 | 13° 41.329 | 43,9 | |
| 1-1 | PM2-1 | 07.10. | Multibeam SES | 08:36 | 54° 54.064 | 13° 37.979 | 43,4 | |
| 1-4 | PM2-2 | 07.10. | Micro-GI Multibeam SES | 09:18 | 54° 54.129 | 132° 35.792 | 43,4 | |

| | | | | | | | | |
|---|---|---|---|---|---|---|---|---|
| 1-1 | PM2-3 | 07.10. | Multibeam SES | 09:48 | 54° 54.115 | 13° 38.495 | 46,6 | |
| 1-1 | PM2-4 | 07.10. | Multibeam SES | 10:24 | 54° 54.435 | 13° 35.696 | 46,4 | |
| 1-1 | PM2-5 | 07.10. | Multibeam SES | 10:54 | 54° 54.489 | 13° 37.950 | 46,4 | |
| 1-1 | PM2-6 | 07.10. | Multibeam SES | 11:24 | 54° 54.454 | 13° 35.761 | 46,4 | |
| 1-1 | PM2-7 | 07.10. | Multibeam SES | 11:50 | 54° 54.529 | 13° 38.536 | 46,5 | |
| 1-1 | PM2-8 | 07.10. | Multibeam SES | 12:19 | 54° 54.593 | 13° 38.536 | 46,5 | |
| 1-1 | PM2-9 | 07.10. | Multibeam SES | 13:08 | 54° 54.945 | 13° 37.840 | 46,6 | |
| 1-5 | 039pre | 07.10. | Micro-GI GI Multibeam SES | 16:10 | 54° 52.749 | 13° 30.244 | 46,0 | |
| 1-5 | 039 | 07.10. | Micro-GI GI Multibeam SES | 17:00 | 54° 54.974 | 13° 34.791 | 46,3 | |
| 1-5 | 040 | 07.10. | Micro-GI GI Multibeam SES | 17:30 | 54° 55.044 | 13° 38.781 | 46,5 | |
| 1-5 | 041 | 07.10. | Micro-GI GI Multibeam SES | 20:00 | 54° 56.633 | 14° 0.200 | 46,0 | |
| 1-5 | 042 | 07.10. | Micro-GI Multibeam SES | 20:42 | 54° 53.804 | 14° 3.677 | 42,4 | |
| 1-5 | 043 | 07.10. | Micro-GI Multibeam SES | 21:02 | 54° 52.447 | 14° 2.144 | 41,8 | |
| 1-5 | 044 | 07.10. | Micro-GI Multibeam SES | 22:19 | 54° 56.40 | 13° 58.355 | 46,1 | |
| 1-5 | 45 | 08.10. | Micro-GI Multibeam SES | 00:13 | 54° 59.219 | 13° 45.220 | 46,5 | |
| 1-5 | 046 | 08.10. | Micro-GI Multibeam SES | 03:29 | 54° 58.400 | 13° 17.878 | 45,6 | |
| 1-5 | 047 | 08.10. | Micro-GI Multibeam SES | 07:14 | 54° 57.564 | 13° 50.056 | 46,5 | |
| 1-5 | 048 | 08.10. | Micro-GI Multibeam SES | 07:33 | 54° 56.359 | 13° 49.436 | 46,4 | |
| 1-5 | 049 | 08.10. | Micro-GI Multibeam SES | 10:08 | 54° 56.204 | 13° 26.519 | | |
| 1-5 | 050 | 08.10. | Micro-GI Multibeam SES | 11:56 | 54° 50.710 | 13° 15.698 | 43,5 | |
| 1-5 | 051 | 08.10. | Micro-GI Multibeam SES | 12:54 | 54° 47.481 | 13° 21.988 | 42,5 | |
| 1-5 | 052 | 08.10. | Micro-GI Multibeam SES | 14:10 | 54° 47.825 | 13° 32.164 | 43,4 | |
| 1-5 | 053 | 08.10. | Micro-GI Multibeam SES | 16:33 | 54° 36.388 | 13° 29.594 | 20,0 | |
| 1-5 | 054 | 08.10. | Micro-GI Multibeam SES | 16:46 | 54° 36.427 | 13° 31.371 | 21,9 | |
| 1-5 | 055 | 08.10. | Micro-GI Multibeam SES | 17:19 | 54° 36.935 | 13° 35.698 | 25,7 | |
| 1-5 | 056 | 08.10. | Micro-GI Multibeam SES | 18:59 | 54° 45.210 | 13° 35.971 | 41,0 | |
| 1-5 | 057 | 08.10. | Micro-GI Multibeam SES | 19:14 | 54° 45.197 | 13° 33.970 | 41,0 | |
| 1-5 | 058 | 08.10. | Micro-GI Multibeam SES | 20:57 | 54° 36.509 | 13° 32.109 | 22,4 | |
| 1-5 | 059 | 08.10. | Micro-GI Multibeam SES | 22:23 | 54° 36.440 | 13° 44.209 | 26,0 | |
| 1-5 | 060 | 08.10. | Micro-GI Multibeam SES | 23:04 | 54° 29.836 | 13° 45.457 | 17,3 | |
| 1-5 | 061 | 09.10. | Micro-GI Multibeam SES | 00:55 | 54° 28.136 | 13° 36.656 | 14,2 | |
| 1-5 | 062 | 09.10. | Micro-GI Multibeam SES | 01:45 | 54° 25.550 | 13° 37.682 | 14,0 | |
| 1-5 | 063 | 09.10. | Micro-GI Multibeam SES | 02:31 | 54° 28.391 | 13° 37.147 | 15,1 | |
| 1-5 | 064 | 09.10. | Micro-GI Multibeam SES | 03:40 | 54° 24.404 | 13° 42.390 | 14,4 | |
| 1-5 | 065 | 09.10. | Micro-GI Multibeam SES | 04:43 | 54° 29.115 | 13° 38.435 | 15,1 | |
| 1-5 | 066 | 09.10. | Micro-GI Multibeam SES | | 54° 32.230 | 13° 55.740 | | |
| 1-7 | NS2-Transit | 10.10. | Multibeam SES | 08:29 | 54° 30.728 | 14° 3.371 | 17,3 | Transit to the Nordstream Pipeline, SES operating in Beam steering mode at 4 kHz with three beams at -12°,0° adn 12° |
| 1-7 | NS2-1 | 10.10. | Multibeam SES | 09:46 | 54° 30.45 | 14° 02.54 | 17,0 | Multiple corssings of the Nordstream Pipeline with MBES and SES (Beam steering mode 4kHz, 3 beams -12°,0°,12°), please note that the name is missleading: The Nordstream Pipeline was surveyed (NOT Nordstream2) |

| | | | | | | | | |
|---|---|---|---|---|---|---|---|---|
| 1-8 | 067_pre | 10.10. | Micro-GI Multibeam SES | 12:28 | 54° 31.58 | 14° 08.73 | 18,0 | Mammal watching started 11:32, Soft start procedure started 12:28, 8ch MaMuCS started recording with slight delay of about 100 shots, SES switched back to Multifrequency mode at 5, 10 , 15 kHz, Birds flying at 0.7m |
| 1-8 | 067 | 10.10. | Micro-GI Multibeam SES | 12:47 | 54° 32.201 | 14° 8.429 | 18,2 | Birds at 0.7m |
| 1-8 | 068 | 10.10. | Micro-GI Multibeam SES | 13:29 | 54° 32.791 | 14° 0.272 | 18,0 | Birds at 0.7 m |
| 1-8 | 069 | 10.10. | Micro-GI Multibeam SES | 16:29 | 54° 39.487 | 14° 36.782 | 46,8 | Change of bird depth form 0.7m to 1m at FFN 6046 at 19:11 |
| 1-8 | 070 | 10.10. | Micro-GI Multibeam SES | 19:28 | 54° 40.050 | 15° 2.641 | 57,0 | Birds at 1m |
| 1-8 | 071 | 10.10. | Micro-GI Multibeam SES | 20:54 | 54° 35.04 | 15° 11.49 | 51,3 | Birds at 1m |
| 1-8 | 072 | 11.10. | Micro-GI Multibeam SES | 00:39 | 54° 42.087 | 15° 41.187 | 66,4 | Birds at 1m |
| 1-8 | 073 | 11.10. | Micro-GI Multibeam SES | 03:26 | 54° 53.214 | 15° 54.311 | 72,3 | To fix compressor/gun problems a loop was done at 04:21- 04:34 (FFN14275-14470), general technical situation problematic: Tailbuoy flipped and low pressure at beginning of profile (125 bar before 04:21, 140 after), SES window jumpy, thus recording length had to be limited to 100m and the start of the window was shifted to gain sufficient sediment penetration, Birds at 1m |
| 1-8 | 074 | 11.10. | Micro-GI Multibeam SES | 09:52 | 55° 22.44 | 16° 01.87 | 86,5 | Birds at 1 m until 10:30, then 0.7 m |
| 1-8 | 075 | 11.10. | Micro-GI Multibeam SES | 16:40 | 55° 37.444 | 15° 9.104 | 74,4 | Birds at 0.7 m |
| 1-8 | 076 | 11.10. | Micro-GI Multibeam SES | 17:17 | 55° 39.801 | 15° 6.392 | 69,4 | Birds at 0.7 m |
| 1-8 | 077 | 11.10. | Micro-GI Multibeam SES | 21:39 | 55° 22.11 | 14° 44.86 | 62,0 | Birds at 0.7 m |
| 1-8 | 078 | 11.10. | Micro-GI Multibeam SES | 22:50 | 55° 27.598 | 14° 41.798 | 68,5 | Birds at 0.7 m |
| 1-8 | 079 | 11.10. | Micro-GI Multibeam SES | 23:36 | 55° 30.094 | 14° 45.762 | 67,0 | Birds at 0.7 m |
| 1-8 | 080 | 11.10. | Micro-GI Multibeam SES | 23:54 | 55° 29.11 | 14° 47.82 | 70,0 | Birds at 0.7 m |
| 1-8 | 081 | 12.10. | Micro-GI Multibeam SES | 00:37 | 55° 26.725 | 14° 45.130 | 70,0 | Birds at 0.7 m |
| 1-8 | 082 | 12.10. | Micro-GI Multibeam SES | 01:29 | 55° 29.507 | 14° 49.810 | 60,0 | Birds at 0.7 m |
| 1-8 | 083 | 12.10. | Micro-GI Multibeam SES | 02:14 | 55° 26.853 | 14° 50.503 | 72,0 | Birds at 0.7 m |
| 1-8 | 084 | 12.10. | Micro-GI Multibeam SES | 02:49 | 55° 28.971 | 14° 51.962 | 62,0 | Birds at 0.7 m |
| 1-7 | 085 | 12.10. | Multibeam SES | 03:29 | 55° 26.398 | 14° 52.856 | 51,4 | |
| 1-7 | 086 | 12.10. | Multibeam SES | 03:40 | 55° 26.146 | 14° 51.453 | 72,4 | |
| 6-2 | 087-pre | 12.10. | Micro-GI Multibeam SES Hydro | 09:20 | | | 70,4 | softstart GI gun |
| 6-2 | 087 | 12.10. | Micro-GI Multibeam SES Hydro | 09:27 | 55° 39.411 | 15° 4.613 | 70,4 | |
| 6-2 | 088 | 12.10. | Micro-GI Multibeam SES Hydro | 09:50 | 55° 40.800 | 15° 3.567 | 65,0 | |
| 6-2 | 089 | 12.10. | Micro-GI Multibeam SES Hydro | 10:20 | 55° 38.840 | 15° 1.134 | 74,0 | change depth window of SES (20m +100m) |
| 6-2 | 090 | 12.10. | Micro-GI Multibeam SES Hydro | 11:13 | 55° 35.013 | 15° 3.187 | 78,0 | |

| | | | | | | | | |
|---|---|---|---|---|---|---|---|---|
| 6-2 | 091 | 12.10. | Micro-GI Multibeam SES Hydro | 11:43 | | | | |
| 6-2 | 092 | 12.10. | Micro-GI Multibeam SES Hydro | 14:04 | 55° 24.011 | 15° 6.69 | 80,8 | |
| 6-2 | 093 | 12.10. | Micro-GI Multibeam SES Hydro | 14:19 | 55° 24.102 | 15° 7.922 | 82,0 | |
| 6-2 | 095 | 12.10. | Micro-GI Multibeam SES Hydro | 15:57 | 55° 28.928 | 15° 15.697 | 80,2 | |
| 6-2 | 096 | 12.10. | Micro-GI Multibeam SES Hydro | 17:18 | 55° 22.710 | 15° 10.328 | 85,8 | |
| 6-2 | 097 | 12.10. | Micro-GI Multibeam SES Hydro | 18:21 | 55° 19.94 | 15° 02.63 | 70,0 | |
| 6-2 | 098 | 12.10. | Micro-GI Multibeam SES Hydro | 19:10 | 55° 16.853 | 15° 6.941 | 71,8 | |
| 6-2 | 099 | 12.10. | Micro-GI Multibeam SES Hydro | 19:47 | 55° 14.15 | 15° 05.17 | 59,0 | |
| 6-2 | 100 | 12.10. | Micro-GI Multibeam SES Hydro | 20:22 | 55° 14.17 | 15° 10.32 | 61,0 | |
| 6-2 | 101 | 12.10. | Micro-GI Multibeam SES Hydro | 21:07 | 55° 10.788 | 15° 12.602 | 65,0 | |
| 6-2 | 102 | 12.10. | Micro-GI Multibeam SES Hydro | 21:45 | 55° 12.63 | 15° 16.70 | 46,0 | |
| 6-2 | 103 | 12.10. | Micro-GI Multibeam SES Hydro | 23:18 | 55° 5.196 | 15° 15.808 | 67,4 | |
| 6-2 | 104 | 13.10. | Micro-GI Multibeam SES Hydro | 01:59 | 55° 11.809 | 15° 35.615 | 94,4 | |
| 6-2 | 105 | 13.10. | Micro-GI Multibeam SES Hydro | 03:59 | 55° 1.703 | 15° 39.358 | 80,0 | |
| 6-2 | 106 | 13.10. | Micro-GI Multibeam SES Hydro | 09:43 | 54° 40.30 | 15° 02.19 | 57,0 | |
| 6-2 | 107 | 13.10. | Micro-GI Multibeam SES Hydro | 11:25 | 54° 46.425 | 14° 50.991 | 56,1 | |
| 6-2 | 108 | 13.10. | Micro-GI Multibeam SES Hydro | 14:34 | 54° 38.056 | 14° 25.484 | 31,1 | |
| 6-2 | Calibration | 13.10. | Micro-GI Multibeam SES Hydro | 18:02 | 54° 38.239 | 13° 52.032 | 24,6 | Change to profile Calibration; MaMUCS range changed to 10V; Gain on MaMUCS changed to 1; Speed of the ship has reduced; calibration begins; Birds set to 5 m depth |

## 7 Data and Sample Storage and Availability

Metadata and CSR were submitted to BSH/DOD after the cruise. Raw seismic and hydroacoustic data are stored in the data base of the Research Group "Marine Technology – Environmental Research" at Bremen University. Additionally, these data are stored in the central Green IT-Housing-Center of the University Bremen on servers belonging to the research group. All published data will be made freely available via PANGAEA immediately after publication. All data are made available on request after a moratorium of 3 years.

**Table 7.1** Overview of data availability

| Type | Database | Available | Free Access | Contact |
|---|---|---|---|---|
| Multichannel seismic and hydroacoustic data, CTD | Uni Bremen | 20.10.2020 | 20.08.2023 | Volkhard Spiess FB5, Uni Bremen tschwenk@uni-bremen.del |

## 8 Acknowledgements

The advisors thanks captain and crew for the excellent support during the cruise and making the cruise possible under this special circumstances. The students thank that the hybrid version of this excursion was possible to continue the curriculum without delay.

## 9 References

Al Hseinat, M., & Hübscher, C., 2017. Late Cretaceous to recent tectonic evolution of the North German Basin and the transition zone to the Baltic Shield/southwest Baltic Sea. Tectonophysics 708, 28-55.

Andrén, E., Andrén, T., & Kunzendorf, H., 2000. Holocene history of the Baltic Sea as a background for assessing records of human impact in the sediments of the Gotland Basin. The Holocene 10(6), 687-702.

Andrén, T., Björck, S., Andrén, E., Conley, D., Zillén, L., & Anjar, J., 2011. The development of the Baltic Sea Basin during the last 130 ka. In The Baltic Sea Basin. Springer, Berlin, Heidelberg, pp. 75-97

Bayer, U., Scheck, M., Rabbel, W., Krawczyk, C. M., Götze, H. J., Stiller, M. & Kuder, J., 1999. An integrated study of the NE German Basin. Tectonophysics 314(1-3), 285-307.

Bennike, O., & Jensen, J. B., 2011. Postglacial, relative shore-level changes in Lillebælt, Denmark. Geological Survey of Denmark and Greenland (GEUS) Bulletin 23, 37-40.

Bennike, O., & Jensen, J. B., 2013. A Baltic Ice Lake lowstand of latest Allerød age in the Arkona basin, southern Baltic Sea. Geological Survey of Denmark and Greenland (GEUS) Bulletin 28, 17-20.

Bennike, O., Andreasen, M. S., Jensen, J. B., Moros, M., & Noe-Nygaard, N., 2012. Early Holocene sea-level changes in Øresund, southern Scandinavia. Geological Survey of Denmark and Greenland (GEUS) Bulletin 26, 29-32.

Bennike, O., Jensen, J. B., Lemke, W., Kuijpers, A., & Lomholt, S., 2004. Late-and postglacial history of the Great Belt, Denmark. Boreas 33(1), 18-33.

Berglund, B. E., Sandgren, P., Barnekow, L., Hannon, G., Jiang, H., Skog, G., & Yu, S. Y., 2005. Early Holocene history of the Baltic Sea, as reflected in coastal sediments in Blekinge, southeastern Sweden. Quaternary International 130(1), 111-139.

Blondel, P., & Murton, B. J. (1997). Handbook of seafloor sonar imagery (Vol. 7). Wiley, Chichester.

Björck, S., 1995. A review of the history of the Baltic Sea, 13.0-8.0 kaBP. Quaternary International 27, 19-40.

Björck, S., 2008. The late Quaternary development of the Baltic Sea basin. In: The BACC Author Team (eds) Assessment of climate change for the Baltic Sea Basin. Springer, Berlin, Heidelberg, 398-407.

Clausen, O. R., & Pedersen, P. K., 1999. Late Triassic structural evolution of the southern margin of the Ringkøbing-Fyn High, Denmark. Marine and Petroleum Geology 16(7), 653-665.

De Moustier, C., 1986. Beyond bathymetry: Mapping acoustic backscattering from the deep seafloor with Sea Beam. The Journal of the Acoustical Society of America 79(2), 316-331.

Erlstrom, M., Thomas, S. A., Deeks, N., and Sivhed, U., 1997. Structure and tectonic evolution of the Tornquist Zone and adjacent sedimentary basins in Scania and the southern Baltic Sea area. Tectonophysics 271, no. 3-4, 202-220.

Grassmann, S., Cramer, B., Delisle, G., Messner, J., & Winsemann, J., 2005. Geological history and petroleum system of the Mittelplate oil field, Northern Germany. International Journal of Earth Sciences 94(5-6), 979-989.

Houmark-Nielsen, M., & Henrik Kjær, K., 2003. Southwest Scandinavia, 40–15 kyr BP: palaeogeography and environmental change. Journal of Quaternary Science 18(8), 769-786.

Houmark-Nielsen, M. (2010). Extent, age and dynamics of Marine Isotope Stage 3 glaciations in the southwestern Baltic Basin. Boreas 39(2), 343-359.

Hübscher, C., Hansen, M. B., Trinanes, S. P., Lykke-Andersen, H., & Gajewski, D., 2010. Structure and evolution of the Northeastern German Basin and its transition onto the Baltic Shield. Marine and petroleum geology 27(4), 923-938.

Ignatius, H., Axberg, S., Niemistö, L., & Winterhalter, B., 1981. Quaternary geology of the Baltic Sea. The Baltic Sea 54, 104.

International Hydrographic Organisation (IHO). (2008). IHO Standards for Hydrographic Surveys, 5th Edition, February 2008 Special Publication No. 44. International Hydrographic

Bureau. Monaco

Innomar (2009, June). SES-2000 Narrow-Beam Parametric Sub-Bottom Profilers – User's Guide.

Jackson, D. R., Winebrenner, D. P., & Ishimaru, A., 1986. Application of the composite roughness model to high-frequency bottom backscattering. The Journal of the Acoustical Society of America 79(5), 1410-1422.

Jakobsson, M., Gyllencreutz, R., Mayer, L. A., Dowdeswell, J. A., Canals, M., Todd, B. J. & Larter, R. D., 2016. Mapping submarine glacial landforms using acoustic methods. Geological Society, London, Memoirs 46(1), 17-40.

Jöns, H., 2011. Settlement development in the shadow of coastal changes–case studies from the Baltic Rim. In: The Baltic Sea Basin. Springer, Berlin, Heidelberg, pp. 301-336.

Jones, E. J. W., 1999. Marine Geophysics. Wiley, New York

Kortekaas, M., Murray, A. S., Sandgren, P., & Björck, S., 2007. OSL chronology for a sediment core from the southern Baltic Sea: a continuous sedimentation record since deglaciation. Quaternary Geochronology 2(1-4), 95-101.

Kossow, D., Krawczyk, C., McCann, T., Strecker, M., & Negendank, J. F., 2000. Style and evolution of salt pillows and related structures in the northern part of the Northeast German Basin. International Journal of Earth Sciences 89(3), 652-664.

Krauss, M. & Mayer, P., 2004. Das Vorpommern-Storungssystem und seine regionale Einordnung zur Transeuropaischen Storung. Zeitschrift fur Geologische Wissenschaften, 32(2/4), 227-234.

Krauss, M., 1994. The tectonic structure below the southern Baltic Sea and its evolution. Zeitschrift Geologische Wissenschaften, 22, 19-32.

Lambeck, K., & Chappell, J., 2001. Sea level change through the last glacial cycle. Science 292(5517), 679-686.

Lambeck, K., Purcell, A., Zhao, J., & Svensson, N. O., 2010. The Scandinavian ice sheet: from MIS 4 to the end of the last glacial maximum. Boreas 39(2), 410-435.

Lemke, W., Jensen, J. B., Bennike, O., Endler, R., Witkowski, A., & Kuijpers, A., 2001. Hydrographic thresholds in the western Baltic Sea: Late Quaternary geology and the Dana River concept. Marine Geology 176(1-4), 191-201.

Lemke, W., Jensen, J. B., Bennike, O., Witkowski, A., & Kuijpers, A., 1999. No indication of a deeply incised Dana River between Arkona Basin and Mecklenburg Bay. Baltica,12, 66-70.

Lurton, X., 2002. An introduction to underwater acoustics: principles and applications. Springer Science & Business Media, Berlin, Heidelberg.

Maystrenko, Y., Bayer, U., Brink, H. J., & Littke, R., 2008. The Central European basin system–

an overview. In: Dynamics of complex intracontinental basins. Springer, Berlin, Heidelberg, pp. 16-34.

Norbit (n.d.). NORBIT – iWBMSe Entry-Level Turnkey Multibeam Sonar System [Fact sheet]

Pharaoh, T. C., England, R. W., Verniers, J., & Żelaźniewicz, A., 1997. Introduction: geological and geophysical studies in the Trans-European Suture Zone. Geological Magazine 134(5), 585-590.

Reson (2006, February 13). SeaBat 7125 Operator's Manual.

Rosentau, A., Bennike, O., Uscinowicz, S., & Miotk-Szpiganowicz, G., 2017. The Baltic Sea Basin. In: Submerged landscapes of the European continental shelf: quaternary paleoenvironments. Wiley, Chichester, 103-133.

Schlüter, H. U., Jürgens, U., Binot, F., & Best, G., 1998. The importance of geological structures as natural sources of potentially hazardous substances in the southern part of the Baltic Sea. ZEITSCHRIFT FUR ANGEWANDTE GEOLOGIE 44, 26-32.

Sohlenius, G., Emeis, K. C., Andrén, E., Andrén, T., & Kohly, A., 2001. Development of anoxia during the Holocene fresh–brackish water transition in the Baltic Sea. Marine Geology 177(3-4), 221-242.

Sohlenius, G., Sternbeck, J., Andrén, E., & Westman, P., 1996. Holocene history of the Baltic Sea as recorded in a sediment core from the Gotland Deep. Marine Geology 134(3-4), 183-201.

Sohlenius, G., & Westman, P., 1998. Salinity and redox alternations in the northwestern Baltic proper during the late Holocene. Boreas 27(2), 101-114.

Svendsen, J. I., Alexanderson, H., Astakhov, V. I., Demidov, I., Dowdeswell, J. A., Funder, S., & Hubberten, H. W., 2004. Late Quaternary ice sheet history of northern Eurasia. Quaternary Science Reviews 23(11-13), 1229-1271.

Urban, H. G. (2002). Handbuch der Wasserschalltechnik. Eigenverl. STN Atlas Elektronik GmbH.

Urick, R. J., 1975. Principles of underwater sound-2. MacGraw-Hill Book, New York

Van Wees, J. D., Stephenson, R. A., Ziegler, P. A., Bayer, U., McCann, T., Dadlez, R., & Scheck, M., 2000. On the origin of the southern Permian Basin, Central Europe. Marine and Petroleum Geology 17(1), 43-59.

Walker, M., Johnsen, S., Rasmussen, S. O., Popp, T., Steffensen, J. P., Gibbard, P. & Cwynar, L. C., 2009. Formal definition and dating of the GSSP (Global Stratotype Section and Point) for the base of the Holocene using the Greenland NGRIP ice core, and selected auxiliary records. Journal of Quaternary Science 24(1), 3-17.

Winterhalter, B., 1992. Late-Quaternary stratigraphy of Baltic Sea basins—a review. Bulletin of the Geological Society of Finland 64(Part 2), 189-194.

Winterhalter, B. O. R. I. S., Flodén, T., Ignatius, H., Axberg, S., & Niemistö, L., 1981. Geology of the Baltic Sea. In: Elsevier Oceanography Series (Vol. 30, pp. 1-121). Elsevier, Amsterdam.

Yu, S. Y., Berglund, B. E., Sandgren, P., & Lambeck, K., 2007. Evidence for a rapid sea-level rise 7600 yr ago. Geology 35(10), 891-894.

# 11 Appendices

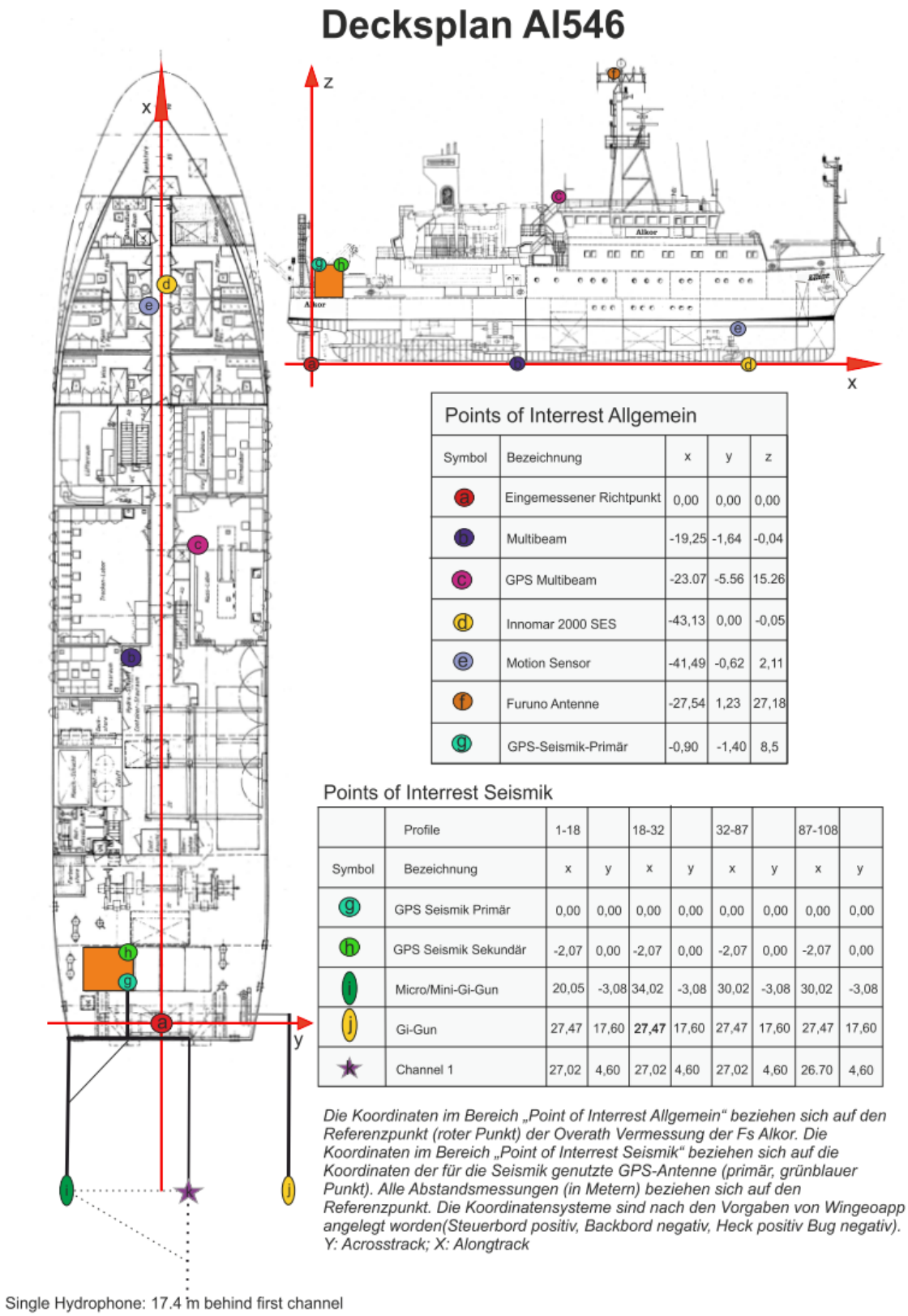


Points of Interrest Allgemein

| Symbol | Bezeichnung | x | y | z |
|---|---|---|---|---|
| a | Eingemessener Richtpunkt | 0,00 | 0,00 | 0,00 |
| b | Multibeam | -19,25 | -1,64 | -0,04 |
| c | GPS Multibeam | -23.07 | -5.56 | 15.26 |
| d | Innomar 2000 SES | -43,13 | 0,00 | -0,05 |
| e | Motion Sensor | -41,49 | -0,62 | 2,11 |
| f | Furuno Antenne | -27,54 | 1,23 | 27,18 |
| g | GPS-Seismik-Primär | -0,90 | -1,40 | 8,5 |

Points of Interrest Seismik

| | Profile | 1-18 | | 18-32 | | 32-87 | | 87-108 | |
|---|---|---|---|---|---|---|---|---|---|
| Symbol | Bezeichnung | x | y | x | y | x | y | x | y |
| g | GPS Seismik Primär | 0,00 | 0,00 | 0,00 | 0,00 | 0,00 | 0,00 | 0,00 | 0,00 |
| h | GPS Seismik Sekundär | -2,07 | 0,00 | -2,07 | 0,00 | -2,07 | 0,00 | -2,07 | 0,00 |
| i | Micro/Mini-Gi-Gun | 20,05 | -3,08 | 34,02 | -3,08 | 30,02 | -3,08 | 30,02 | -3,08 |
| j | Gi-Gun | 27,47 | 17,60 | **27,47** | 17,60 | 27,47 | 17,60 | 27,47 | 17,60 |
| ★ | Channel 1 | 27,02 | 4,60 | 27,02 | 4,60 | 27,02 | 4,60 | 26.70 | 4,60 |

*Die Koordinaten im Bereich „Point of Interrest Allgemein" beziehen sich auf den Referenzpunkt (roter Punkt) der Overath Vermessung der Fs Alkor. Die Koordinaten im Bereich „Point of Interrest Seismik" beziehen sich auf die Koordinaten der für die Seismik genutzte GPS-Antenne (primär, grünblauer Punkt). Alle Abstandsmessungen (in Metern) beziehen sich auf den Referenzpunkt. Die Koordinatensysteme sind nach den Vorgaben von Wingeoapp angelegt worden(Steuerbord positiv, Backbord negativ, Heck positiv Bug negativ). Y: Acrosstrack; X: Alongtrack*

*App 1: Deck plan and geometry of sensors and sources*